

The Optical Properties of Gravitational Lens Galaxies as a Probe of Galaxy Structure and Evolution¹

C. R. Keeton, C. S. Kochanek, and E. E. Falco
Harvard-Smithsonian Center for Astrophysics, MS-51
60 Garden Street
Cambridge, MA 02138

ABSTRACT

We combine photometry and lens modeling to study the properties of 17 gravitational lens galaxies between $z = 0.1$ and ~ 1 . Most of the lens galaxies are passively evolving early-type galaxies, with a few spirals. The colors, scale lengths, and ellipticities of lens galaxies are similar to those of the general population of early-type galaxies, although there may be a deficit of apparently round lens galaxies produced by the inclination dependence of lensing cross sections. The projected mass distributions are aligned with the projected light distributions to $\lesssim 10^\circ$, except in the presence of a strong external tidal perturbation, suggesting that dark matter halos have orbits that are significantly modified by interactions with the baryonic component and are not far out of alignment with the stars. Lens galaxies obey image separation/lens luminosity correlations analogous to the Faber-Jackson and Tully-Fisher relations, which are consistent with standard dark matter lens models. The lens galaxy mass-to-light ratios decrease with redshift as $d(\log M/L_B)/dz = -0.3 \pm 0.1$ (-0.5 ± 0.1) for $\Omega_0 = 1$ (0.1), thus providing direct evidence of passive evolution for a sample of early-type galaxies in low-density environments. The evolution-corrected mass-to-light ratios are generally larger than predicted by constant M/L dynamical models, although there is significant scatter; with improved photometry, lens galaxy mass-to-light ratios would better distinguish between constant M/L and dark matter models. These conclusions are limited primarily by the quality of lens galaxy photometry.

Subject headings: gravitational lensing – galaxies: fundamental parameters – galaxies: evolution

¹Based on observations made with the NASA/ESA Hubble Space Telescope, obtained at the Space Telescope Science Institute, which is operated by AURA, Inc., under NASA contract NAS5-26555.

1. Introduction

Although knowledge of the distribution of galaxies in color, luminosity, structure, and redshift is growing rapidly (e.g. Griffiths et al. 1994; Lilly et al. 1995; Schade et al. 1995; Lin et al. 1996, 1997; Ellis 1997) there is still little direct information on the masses of intermediate-redshift galaxies. As a result, most physical inferences about galaxy populations above $z \sim 0.1$ (such as evolution rates) remain critically dependent on modeling the relations between a galaxy’s luminosity and its stellar or total mass. For nearby galaxies, masses can be estimated by combining a dynamical model with well-defined correlations between luminosities, scale lengths, and velocities such as the Faber-Jackson (Faber & Jackson 1976) and Tully-Fisher (Tully & Fisher 1977) relations and the fundamental plane of elliptical galaxies (e.g. Djorgovski & Davis 1987; Dressler et al. 1987). These relations have recently been extended to $z \sim 0.5$ to study galaxy evolution (e.g. van Dokkum & Franx 1996; Kelson et al. 1997), but the observations are difficult because of the need for spectra with high resolution and high signal-to-noise ratio. Other studies, both spectroscopic (e.g. Bender, Ziegler & Bruzual 1996) and photometric (e.g. Pahre, Djorgovski & de Carvalho 1996; Schade et al. 1996, 1997; Stanford, Eisenhardt & Dickinson 1997) have also found evidence for galaxy evolution out to $z \sim 1$. All these results apply only to ensembles of galaxies that are in high-density, cluster environments, where evolution may or may not be typical (see Stanford et al. 1997).

There is, however, one population of galaxies whose masses can be determined individually with high precision at any redshift, and which are found in a wide range of environments – gravitational lens galaxies. The mass enclosed by the images of a four-image lens is determined in a model-independent way with an internal uncertainty of only a few percent (e.g. Kochanek 1991a; Wambsganss & Paczyński 1994). The full range of cosmological models, plausible external perturbations due to nearby objects (e.g. Keeton, Kochanek & Seljak 1997), and large-scale structure (e.g. Bar-Kana 1996; Wambsganss et al. 1997) can change the masses by $\lesssim 20\%$. Such precision is better than that achieved by dynamical studies of individual nearby galaxies, and far exceeds the precision possible for galaxies at intermediate redshifts using dynamical methods. Hence measuring masses via lensing allows us to replace difficult measurements and analyses of high-precision dynamical observations with simpler observations of source and lens redshifts and lens galaxy photometry, making it much easier to study physical properties such as the evolution of mass-to-light ratios.

Lensing also offers a way to directly probe the mass distributions of distant galaxies, and to compare them with their light distributions. Lens models and statistics (e.g. Maoz & Rix 1993; Kochanek 1995, 1996a; Grogin & Narayan 1996) suggest that lens galaxies are

not well described by constant mass-to-light ratio models and instead require dark (roughly isothermal) halos, in agreement with results from stellar dynamics and X-ray observations (e.g. Fabbiano 1989; Rix et al. 1997). Lens models also suggest that the quadrupole shapes of the mass and light distributions need not be the same (see Keeton et al. 1997; Jackson, Nair & Browne 1997), which is consistent with models of polar-ring galaxies and X-ray galaxies indicating that dark halos can be significantly flatter than the light (e.g. Sackett et al. 1994; Buote & Canizares 1994, 1996; also see the review by Sackett 1996).

We must bear in mind, however, that the lens galaxies are a biased sample of galaxies. First, the lens galaxy sample preferentially selects massive galaxies, because they are more likely to lens background objects. For example, with an $\alpha = -1$ Schechter (1976) luminosity function $dn/dL \propto (L/L_*)^{-1} \exp(-L/L_*)$, and a dark matter lens model for which the lensing cross section scales as L (e.g. Turner, Ostriker & Gott 1984), the luminosity function of lens galaxies is roughly $dn/dL \propto \exp(-L/L_*)$. In other words, the lensing cross section filters the divergent (by number) population of low-luminosity galaxies out of the lens galaxy sample. The need to resolve the multiple images produced by a lens adds a further bias against low-mass galaxies. Taken together, these mass biases mean that lens galaxies are a poor probe of the “faint blue galaxies” responsible for many of the interpretation problems in galaxy number count models (e.g. Ellis 1997). The mass biases are also biases for early-type galaxies over late-type galaxies; because of their smaller masses, spiral galaxies are expected to account for only 10–20% of gravitational lenses (e.g. Turner et al. 1984; Fukugita & Turner 1991; Kochanek 1993a, 1996a; Maoz & Rix 1993; Keeton & Kochanek 1997b).

The average lens galaxy is expected to be flatter than the average galaxy (see Kochanek 1996b; King & Browne 1996; Keeton et al. 1997; Jackson et al. 1997), in part because the efficiency of flattened galaxies as lenses is maximized when they are viewed edge-on (Kochanek 1996b; Keeton & Kochanek 1997b). Despite the “inclination bias,” the lens galaxy sample is not strongly biased to include intrinsically flat galaxies, because inclination-averaged lensing cross sections are almost independent of the intrinsic axis ratio (Keeton & Kochanek 1997b). Finally, optically-selected samples are biased against dusty (e.g. Kochanek 1991b, 1996a; Tomita 1996; Falco, Kochanek & Muñoz 1997a; Malhotra, Rhoads & Turner 1997; Perna, Loeb & Bartelmann 1997) and bright (Kochanek 1991b, 1996a) lens galaxies; because of these two effects the lensed quasar sample is unlikely to contain many examples of lensing by spiral galaxies. Statistical models of radio-selected lenses suggest that the optically-selected quasar lens samples may be only $50^{+40}_{-20}\%$ complete (Falco et al. 1997a). The radio-selected lenses should be a fair sample of galaxies by mass, except for the selection against low-mass galaxies created by the need to resolve the lensed images.

Our goal is to assemble a preliminary survey of the optical properties of gravitational lens galaxies, and to establish their utility as probes of the structure and evolution of galaxies between $z = 0.1$ and 1. Our results will be limited by the number of objects available for study, and by the heterogeneity and quality of the available surface photometry. Neither of these problems is fundamental, and a determined observational program could eliminate these restrictions. In §2 we gather the available data and discuss their quality. We describe new surface photometry of Hubble Space Telescope images, discuss photometric corrections used to convert apparent magnitudes to rest-frame luminosities, and present lens models to characterize lens galaxy mass distributions. In §3 we analyze the optical and mass structures of lens galaxies, the colors of lens galaxies, the correlation between image separation and lens luminosity, and lens galaxy mass-to-light ratios and evolution. In §4 we present our conclusions.

2. Lens Galaxy Data

There are now ~ 30 known multiply-imaged gravitational lenses.² In some lenses the sources are so bright that no lens galaxy has been seen (e.g. the doubles 1208+1011 and J03.13, and the quad H 1413+117), and in others we have no way to determine whether the optical emission is due to the source or to the lens (e.g. B 1938+666 and PKS 1830–211). There are, however, 21 lenses where the lens galaxy has been observed, although the quality of the data varies. We have excluded the lens Q 2237+0305 (Huchra et al. 1985), which consists of four images of a quasar produced by the bulge of a nearby ($z = 0.04$) spiral galaxy, because it is difficult to find a luminosity estimate for the bulge that plays the same role as aperture or total magnitudes for the other lens galaxies. We also excluded the lens MG 2016+112 (Lawrence et al. 1984) because it seems to require two lens galaxies at different redshifts and is not well understood (see Nair & Garrett 1997). Finally, we neglected the lenses FSC 10214+4724 (Eisenhardt et al. 1996) and HE 1104–1805 (Wisotski et al. 1993; Courbin, Lidman & Magain 1997a). Thus we are left with 17 lens galaxies, whose optical properties we summarize in Tables 1–4. We are interested in the lens geometries and redshifts (Table 1), the lens galaxy structural parameters (effective radius, ellipticity, and position angle; Table 2), as well as the lens galaxy color (Table 2), total integrated magnitude (Table 3), and magnitude inside the critical radius (Table 4).

Only a few lens galaxies have structural parameters reported in the literature. More have published photometry, but because the defining aperture is usually unspecified it is

²For a summary, see Keeton & Kochanek (1996) or <http://cfa-www.harvard.edu/glensdata>.

difficult to interpret the data. Many of the lenses, however, have been observed with the Hubble Space Telescope (HST); with these observations we were able to make a systematic analysis of lens galaxy structural parameters and magnitudes. We used our own HST data together with data from the HST public archive (see Table 2 for references). For the analysis, we combined each set of cosmic-ray split images by standard procedures and constructed a synthetic PSF with Tiny Tim (v. 4.3, Krist 1997). We then simultaneously modeled the images as a combination of point sources or Gaussians (for the lensed images) and elliptical de Vaucouleurs profiles (for the galaxies). Each model was computed on a three-times oversampled grid relative to the PSF, which itself was modeled on a two-times oversampled grid relative to the images. The model was optimized to derive the structural parameters of the lens galaxy, which could then be used to compute total and aperture magnitudes. Note that we quote HST instrumental magnitudes rather than converting them to “standard” filters (such as *BVRI*). Finally, we used the full covariance matrix of the model fit to derive formal statistical uncertainties (after rescaling the nominal χ^2 to be unity per degree of freedom). Our procedures are similar to those used by the Medium Deep Survey (e.g. Ratnatunga et al. 1995), and for the two lenses found in the MDS survey (HST 12531–2914 and HST 14176+5226) we derive statistically compatible results. We use only de Vaucouleurs fits to the galaxies because isolated exponential disks failed to provide comparably good fits, and the complication of disk+bulge models is unwarranted at present. Several of the galaxies require special discussion:

- B 0218+357: We could not robustly separate the quasar images from the galaxy in the existing data. We used the results from similar modeling by B. McLeod (1997, private communication).
- Q 0142–100 and BRI 0952–0115: In each case the galaxy properties are sensitive to the treatment of the bright quasar images that bracket the galaxy, and the formal statistical uncertainties underestimate the true systematic errors in the profile fits. A blind deconvolution is needed to construct an accurate model of the true PSF simultaneously with the model of the image.
- Q 0957+561: The galaxy parameters are robust, but as in Q 0142–100 and BRI 0952–0115 the model would benefit from a blind deconvolution, particularly to determine the properties of the low surface brightness (lensed) features discovered by Bernstein et al. (1997).
- MG 1131+0456: There appears to be a very low surface brightness optical ring surrounding the lens galaxy. An optical ring was suggested by Hammer et al. (1991), but their detection is far too bright to match the HST images and must have been created by an error in modeling the galaxy profile and the ground-based PSF.

- B 1600+434: Both the HST V and I images have little flux from the galaxy, although the mean structure is readily apparent if we subtract the lensed images and convolve the residual image with a Gaussian to increase the visibility of the low surface brightness galaxy. There are two peaks to the extended emission, one between the two lensed images, and one underneath the fainter radio image (see Jackson et al. 1997). The low signal-to-noise ratio and the complicated structure prevent any sensible model parameter determinations. The shape, orientation, and color were estimated from aperture photometry.
- B 1608+656: In addition to the obvious extended lensed emission (Jackson et al. 1997), there appears to be a faint ring surrounding the entire galaxy, particularly in the I image. Despite its faintness, the emission strongly affects the profile fits, and a reliable determination of the properties of the lens galaxy will require using a lens model to properly subtract the optical ring. In addition, the lens galaxy shows a complicated structure that may indicate that the lensing mass comprises two galaxies or a single galaxy cut by a dust lane (Jackson et al. 1997).
- B 1933+503: As with B 1600+434, the rough appearance of the galaxy is readily apparent after convolving the images with a Gaussian to enhance the low surface brightness features. However, there is far too little flux from the galaxy to do more than crudely estimate an ellipticity, position angle, and aperture magnitude.

Where we could not robustly extract all the desired data, we either made estimates and enclosed them in parentheses in Tables 2–4 to flag them as systematically suspect, or omitted them altogether if we judged them too unreliable. In most cases the effective radius estimate and hence the total magnitude are the most uncertain quantities, while the ellipticity, position angle, color, and aperture magnitude are relatively reliable.

There are several corrections that should be applied to the magnitudes. First, Table 1 gives $E(B - V)$ values for Galactic extinction, estimated from the survey of Stark et al. (1992). The large foreground extinctions for several lens galaxies (notably the radio-selected lenses MG 0414+0534, B 0712+472, and B 1933+503) produce significant color and magnitude corrections that have not previously been taken into account. We corrected colors and magnitudes for Galactic extinction using extinction coefficients computed with $R_V = 3.3$ and the Cardelli, Clayton & Mathis (1989) model for the extinction curve. Note, however, that Tables 2–4 give instrumental colors and magnitudes without extinction corrections.

Second, as indicated by Tables 3–4, the existing observations use a very heterogeneous set of filters. Comparing the observations to one another and to studies of local galaxies

requires converting to a standard wavelength, which can be done by applying photometric corrections including color, K , and evolutionary corrections. We computed the corrections using the spectral evolution models of Bruzual & Charlot (1993), with the Kurucz (1979) model of α Lyrae to define the standard magnitude zero points. Fukugita, Shimasaku & Ichikawa (1995) discuss the normalizations of a wide variety of photometric systems, and Holtzman et al. (1995) discuss the normalization of the HST/WFPC2 photometric bands. We checked our results against those of Guiderdoni & Rocca-Volmerange (1987, 1988) and Poggianti (1997), both of which describe the standard technique.

The photometric corrections introduce several systematic uncertainties into the converted magnitudes: (1) the choice of the galaxy evolution model, in particular the galaxy formation redshift z_f and the initial mass function (IMF); (2) the cosmological model, which enters the models through the galaxy age as a function of redshift; (3) the star formation rates used to describe different morphological types, which we take from Guiderdoni & Rocca-Volmerange (1988); and (4) the synthetic filters used to simulate real photometric filters. We take as our canonical models a Salpeter (1955) IMF for early-type galaxies and a Scalo (1986) IMF for spiral galaxies, with a formation redshift $z_f = 15$ for all galaxies. We use $H_0 = 50 \text{ km s}^{-1} \text{ Mpc}^{-1}$ and consider several discrete values for Ω_0 and λ_0 . We have not attempted to assign formal uncertainties to the photometric corrections, but based on §3.2 below we estimate that the systematic uncertainties (other than from the cosmological model) are a few tenths of a magnitude.

Finally, we characterize the mass distributions of the lens galaxies using dark matter dominated, singular isothermal ellipsoid (SIE) lens models (see Kassiola & Kovner 1993; Kormann, Schneider & Bartelmann 1994ab; Kochanek 1996b; Keeton et al. 1997). We focus on these models because galaxies generally appear to be singular (e.g. Gebhardt et al. 1996) and because stellar dynamical models (e.g. Rix et al. 1997), X-ray galaxies (e.g. Fabbiano 1989), and lens models and statistics (e.g. Maoz & Rix 1993; Kochanek 1995, 1996a; Grogin & Narayan 1996) generally prefer an isothermal profile. Using an ellipsoidal mass distribution allows us to probe the shape of the mass distribution. We use a surface mass density of the form

$$\frac{2\Sigma}{\Sigma_{cr}} = \frac{b}{r\sqrt{1 + \varepsilon \cos 2(\theta - \theta_0)}} \quad (1)$$

where b is the critical radius, ε an ellipticity parameter related to the axis ratio q by $q^2 = (1 - \varepsilon)/(1 + \varepsilon)$, and θ_0 is the orientation angle of the projected ellipsoid quoted as a standard major-axis position angle (measured North through East). The critical surface density for lensing is $\Sigma_{cr} = 2.34h^{-1}(D_l D_s / 2r_H D_{ls}) \times 10^{11} M_\odot / \text{arcsec}^2$, where $r_H = c/H_0$ is the Hubble radius and D_l , D_s , and D_{ls} are angular diameter distances to the lens, to the source, and from the lens to the source, respectively. Formulas for the deflection and

magnification of the SIE model are given in Kassiola & Kovner (1993), Kormann et al. (1994a), and Keeton & Kochanek (1997b). In addition to the SIE model, another useful isothermal model is a singular isothermal sphere plus external shear (SIS+shear) model where the ellipsoidal mass distribution is replaced by the combination of a spherical mass distribution and an external tidal perturbation (e.g. Falco, Gorenstein & Shapiro 1985; Gorenstein, Shapiro & Falco 1988; Kochanek 1991a). For completeness we consider both the SIE and SIS+shear models, and we summarize the model results in Table 5. Note that for the table we have converted the parameter ε to the ellipticity e using $e = 1 - q$ and $q = (1 - \varepsilon)^{1/2}/(1 + \varepsilon)^{1/2}$.

The models we consider have a single source of shear – an ellipsoidal galaxy or an external shear – and Table 5 shows that they generally cannot give a good fit. For many lenses, obtaining a good χ^2 requires a model with two independent shears, such as an ellipsoidal galaxy with an external shear (e.g. Keeton et al. 1997; Witt & Mao 1997), and in at least four cases the external shear can be attributed to a significant tidal perturbation from a nearby cluster, group, or galaxy (MG 0751+2716, Lehár et al. 1997a; Q 0957+561, e.g. Young et al. 1980, Grogin & Narayan 1996; PG 1115+080, e.g. Keeton & Kochanek 1997a, Kundić et al. 1997a, Schechter et al. 1997, Tonry 1997; B 1422+231, e.g. Hogg & Blandford 1994, Kormann et al. 1994b, Kundić et al. 1997b, Tonry 1997). Nevertheless, the single-shear models are useful because they provide fundamental information about the average monopole and quadrupole of the mass. They give a position angle for the mean shear axis that is largely independent both of the mass profile and of the nature of the shear. They also give a robust mass estimate, namely the mass within the critical radius $M = \pi b^2 \Sigma_{cr}$, that is essentially model-independent (e.g. Kochanek 1991a; Wambsganss & Paczyński 1994) and has internal uncertainties of only a few percent (due to uncertainties in b). There is, in addition, a $\lesssim 10\%$ mass uncertainty due to potential fluctuations from large-scale structure (e.g. Bar-Kana 1996; Wambsganss et al. 1997) and to perturbations from nearby galaxies or groups (e.g. Keeton et al. 1997), as well as a small dependence ($\lesssim 10\%$) on the cosmological model through Σ_{cr} .

3. Results

We now combine the optical data and the lens models to survey the properties of lens galaxies. We consider the structures of the mass and light distributions, the colors of lens galaxies, the correlation between lens galaxy luminosity and image separation, and the mass-to-light ratios and evolution of the lens galaxies.

3.1. Lens galaxy structure

We can ask two questions about the structure of lens galaxies. First, because lensing makes it possible to directly probe the mass distribution of lens galaxies, we can ask how the mass and light distributions compare in individual galaxies. We know that their profiles differ from each other, because in early-type galaxies the light roughly follows a de Vaucouleurs (1948) $r^{1/4}$ law, while the mass must be distributed in a more extended halo that is roughly isothermal (e.g. Fabbiano 1989; Maoz & Rix 1993; Kochanek 1995, 1996a; Grogin & Narayan 1996; Rix et al. 1997), but we can ask how the quadrupole structures compare by studying the shapes and orientations of the models and of the light distributions (also see Keeton et al. 1997; Jackson et al. 1997). Second, we can compare the distribution of optical properties for the lens galaxy sample and the general population of early-type galaxies, and thus examine lensing selection effects and biases.

Figure 1 compares the optical and model major-axis PAs of the lens galaxies. With a few exceptions the PAs are the same to $\lesssim 10^\circ$, i.e. either consistent or different by $\lesssim 2-3\sigma$. Two exceptions are MG 0751+2716 (Lehár et al. 1997) and Q 0957+561 (Young et al. 1980), but in these systems the lens galaxy is part of a cluster or group that contributes to the lensing, so it is not surprising that the average quadrupole of the mass is not aligned with the galaxy’s light. In the remaining outlier, MG 1131+0456, the PA of the model closely matches that expected if two nearby galaxies produce a tidal perturbation (Chen, Kochanek & Hewitt 1995). The models appear, then, to be consistent with the hypothesis that in the absence of external tidal perturbations the projected mass is aligned with the projected light, and conversely that large misalignments signal the presence of external tidal perturbations. Note, however, that the alignment of the galaxy with the shear in B 1422+231 (Hogg & Blandford 1994; Kormann et al. 1994b; Impey et al. 1996; Keeton et al. 1997) reminds us that even strong tidal perturbations need not produce large misalignments. If all large misalignments are attributable to external tides, then halos cannot be far out of equilibrium. In addition, halos probably cannot have the flat, nearly prolate shapes predicted by N-body simulations of dissipationless collapse (e.g. Dubinski & Carlberg 1991; Warren et al. 1992) because such halos combined with modestly triaxial luminous galaxies inferred from kinematic misalignment studies (e.g. Franx, Illingworth & de Zeeuw 1991) produce misalignments between the major axes of the luminous galaxy and the dark halo of $\langle\psi\rangle \simeq 16^\circ \pm 19^\circ$ (Romanowsky & Kochanek 1997).

Figure 1 also compares the optical and model ellipticities. Several lenses with large tidal perturbations (Q 0957+561 and B 1422+231) clearly stand out by requiring models significantly flatter than the light, although one (MG 0751+2716) does not. The remaining lenses show no strong correlation between the optical and model ellipticities. The lack of a

correlation is certainly consistent with the local results that mass and luminous axis ratios can differ (e.g. Sackett et al. 1994; Buote & Canizares 1994, 1996; see the review by Sackett 1996). A quantitative interpretation of Figure 1 is not straightforward, however, because the model ellipticity depends on the mass profile, with steeper density profiles requiring larger ellipticities. Still, it appears that galaxy mass distributions are not intrinsically very flat, which is consistent with the fact that we do not see any lenses with the “disk” image geometry – 2 or 3 images off to one side of the lens galaxy center and bracketing the projected disk – that are associated with highly flattened mass distributions (see Keeton & Kochanek 1997b).

Figure 2 compares the optical axis ratios of the lens galaxies to a sample of early-type galaxies in Coma from Jørgensen & Franx (1994). Visually, there appears to be a deficit of both round and flat lens galaxies compared to the Coma sample, both for the optical quasar and radio lens samples. A Kolmogorov-Smirnov (K-S) test of whether the distributions are identical gives a probability of 32%, which indicates that any differences between the two samples are statistically marginal. The observed numbers of 4-image lenses also suggest that on average lens galaxies are flatter than observed galaxies (Kochanek 1996b; King & Browne 1996; Keeton et al. 1997), but this result is significant only at the 1σ confidence level (Kochanek 1996b). Thus at present the statistical evidence that lens galaxies are significantly flatter than regular galaxies is weak. Such an effect could be explained naturally by the lensing inclination bias, which makes flattened lens galaxies likely to be seen edge-on rather than face-on (Keeton et al. 1997; Keeton & Kochanek 1997b) and predicts a $\sim 30\%$ deficit of $e = 0$ lens galaxies. This effect is not strong for very flat galaxies, because optically flat galaxies such as spirals require a significantly rounder dark halo for stability (Ostriker & Peebles 1973). Given that there is no significant difference in the ellipticity distributions of the optical- and radio-selected samples, and that there are few highly flattened systems, it is unlikely that there is a significant contribution from spiral galaxies independent of the inclination bias.

Finally, Figure 3 shows the relation between lens galaxy effective radius and luminosity (for an $\Omega_0 = 1$ cosmology), compared to the correlation for nearby early-types $R_e/R_{e*} = (L/L_*)^a$ with $R_{e*} = (4 \pm 1)h^{-1}$ kpc and $a = 1.2 \pm 0.2$ (e.g. Kormendy & Djorgovski 1989; Rix 1991). The lens galaxies seem to follow the trend, although the dispersion is large. Also, the result is not very robust because the effective radii (and hence also the total magnitudes) are the most uncertain of the optical parameters, and because several of the lens galaxies (MG 0414+0534, MG 1131+0456, and HST 12531–2914) that do have good estimates of R_e lack lens redshifts.

3.2. Lens galaxy colors

The distribution of lens galaxy colors provides a way to type the galaxies, to probe galaxy evolution, and to make photometric redshift estimates. Fourteen lens galaxies have measured colors (see Table 2); Figure 4 compares them to theoretical color evolution curves for various galaxy types. To help compare the colors we have taken the lenses with known lens redshifts and used the color corrections to transform the observed colors to F555W–F814W (roughly $V - I$), as shown in Figure 4 (top right) and Figure 5. In Figure 5 we also indicate the systematic effects in the theoretical color evolution curves related to the IMF, formation redshift, star formation rate, and cosmological model (see §2).

Of the 14 measured colors, 11 are either consistent with or redder than early-type galaxy models. For B 1600+434 the red color is not reliable because it is based on low signal-to-noise data; Jaunsen & Hjorth (1997) suggested from earlier ground-based observations that the color and morphology of the lens galaxy in B 1600+434 are actually more consistent with a spiral galaxy. For other cases (MG 0414+0534, MG 1131+0456, and HST 12531–2914), the significance of the colors depends heavily on the unknown lens redshifts. If they have $z_l \gtrsim 0.8$ their colors are only modestly redder than those of passively evolving early-types. By contrast, if they are at $z_l \lesssim 0.8$ their colors suggest that a sizable fraction of early-type galaxies must contain enough dust to significantly affect their colors; Lawrence et al. (1995) have suggested that this may be the case at least for MG 0414+0534. The possibility of dust in early-type galaxies would have dramatic consequences for galaxy evolution models, which usually assume that early-types have little dust. It would also affect cosmological constraints derived from optically-selected lens statistics (see Kochanek 1996a; Falco et al. 1997a; Malhotra et al. 1997).

The three lenses with colors bluer than those of early-type models are B 0218+357, B 1608+656, and B 1933+503. For B 1608+656 the color is hard to interpret due to strong contamination from the lensed images (especially in I) and to the complicated structure of the galaxy; the model fits give a redder color than the aperture photometry, and neither is very reliable at present. For B 1933+503 the color is based on very low signal-to-noise data and thus is not very reliable. By contrast, for B 0218+357 the blue color seems reliable and suggestive of an Sa galaxy, which is consistent with other observations. B 0218+357 is the smallest-separation lens known, with an image separation $0''.34$ that is typical of expectations for lensing by spirals ($\langle \Delta\theta \rangle \sim 0''.6$, see §3.3), and the lens contains HI and molecular gas (Carilli, Rupen & Yanny 1993; Wiklind & Combes 1995; Combes & Wiklind 1997), all of which provides strong evidence that the lens galaxy is a spiral.

Figure 5 illustrates the effects of varying the stellar population and evolution models in interpreting the colors. Most lens galaxy colors are roughly consistent with passively

evolving early-type galaxies, and not with spiral galaxies, regardless of the parameter choices. The anomalous colors do not weaken this conclusion, because varying the parameters in the plausible direction (decreasing the formation redshift from $z_f = 15$, or increasing the Hubble constant from $H_0 = 50 \text{ km s}^{-1} \text{ Mpc}^{-1}$) tends to make the theoretical colors bluer rather than redder, so a color that is difficult to explain as an early-type galaxy is even more difficult to explain as a spiral galaxy.

3.3. Image separations and lens luminosities

Theoretical models predict correlations between lens luminosities and image separations, which are used in statistical studies to estimate the cosmological model (e.g. Turner et al. 1984; Fukugita & Turner 1991; Kochanek 1993a, 1996a; Maoz & Rix 1993; Falco et al. 1997a; Im, Griffiths & Ratnatunga 1997). Singular isothermal sphere lens models relate the image separation $\Delta\theta$ to the dark matter velocity dispersion σ of the lens galaxy by $\Delta\theta/\Delta\theta_* = (\sigma/\sigma_*)^2(D_{ls}/D_s)$, where $\Delta\theta_* = 8\pi(\sigma_*/c)^2$ is the image separation produced by an L_* galaxy for a source at infinity. The average observed separation is $\langle\Delta\theta\rangle \simeq \Delta\theta_*/2$ (see Kochanek 1993b for general relations). The Faber-Jackson (1976) and Tully-Fisher (1977) relations then relate the lens galaxy’s velocity dispersion to its luminosity via $L/L_* = (\sigma/\sigma_*)^\gamma$, so we expect an image separation/lens luminosity correlation of the form

$$\frac{L}{L_*} = \left(\frac{\Delta\theta}{\Delta\theta_*} \frac{D_s}{D_{ls}} \right)^{\gamma/2}, \quad \text{or} \quad (2)$$

$$M_B = M_{B*} - 1.25 \gamma \log \left(\frac{\Delta\theta}{\Delta\theta_*} \frac{D_s}{D_{ls}} \right). \quad (3)$$

For early-type galaxies, Kochanek’s (1993a, 1996a) estimate of the Faber-Jackson relation based on gravitational lens statistics is consistent with $\gamma = 4$ and yields $\sigma_* = 220 \pm 20 \text{ km s}^{-1}$, which also agrees with dark matter models for the stellar dynamics of ellipticals (Kochanek 1994). For spiral galaxies, Fukugita & Turner’s (1991) estimate of the Tully-Fisher relation is $\gamma \approx 2.6$ and $\sigma_* = 144_{-13}^{+8} \text{ km s}^{-1}$. These velocity dispersions yield characteristic image splittings of $\Delta\theta_*(\text{E/S0}) = 2''.79$ and $\Delta\theta_*(\text{spiral}) = 1''.19$. In other words, for the same luminosity a spiral produces a smaller image separation than an early-type; conversely, for a fixed image separation a spiral must be ~ 2 mag brighter than an early-type. Finally, from galaxy number counts and dynamical models, an L_* galaxy has an absolute B magnitude of $M_{B*} = (-19.7 \pm 0.1) + 5 \log h$ (Efstathiou, Ellis & Peterson 1988).

Figure 6 shows the predicted relations for E/S0 and spiral galaxies, together with the empirical results for lenses with at least one known redshift. The image separations

were taken to be $\Delta\theta = 2b_{SIS}$ with b_{SIS} from Table 5. The rest-frame B luminosities were estimated by using the total magnitudes in Table 3 with the color, K , evolutionary, and Galactic extinction corrections described in §2. Some of the magnitudes in Table 3 are estimates of the total integrated magnitude, and we indicate these with filled points in Figure 6. Other magnitudes are only aperture magnitudes, which we indicate with open points. Note that we have included B 1600+434 both as an early-type and a spiral galaxy; the main difference is the value of $\Delta\theta_*$ used in the normalization of the image separation. In general, the data show the expected correlation, although there are a few lenses that need special discussion:

- MG 0414+0534: As with conclusions about the lens galaxy’s color (§3.2), conclusions about its luminosity/image separation relation depend strongly on the lens redshift. If the lens has $z_l \gtrsim 0.8$ (the upper end of the dotted curves in Figure 6), its color, luminosity, and image splitting are all roughly consistent with passively evolving early-type models. Note that without the correction for Galactic extinction, the lens galaxy would appear anomalously red and faint even at $z_l \gtrsim 0.8$.
- B 1600+434: Jaunsen & Hjorth (1997) proposed from ground-based images that the lens galaxy is a spiral, and the HST images reveal a structure that is difficult to interpret but is not inconsistent with a spiral (Jackson et al. 1997). However, Figure 6 shows that when treated as a spiral the lens is underluminous by ~ 2 mag, while when treated as an early-type it sits significantly closer to the trend. Its color (see §3.2) and low luminosity seem anomalous for a spiral, but they are hard to interpret given the existing low signal-to-noise data.
- B 1608+656 and B 1933+503: The colors, although very uncertain, seemed to be more consistent with spiral galaxy models than with early-type models (§3.2). The luminosities and image separations, however, are consistent with the early-type correlation and not with the spiral correlation. Better optical observations (including infrared observations) and lens models are needed to properly interpret these systems.
- MG 0751+2716, PG 1115+080, and B 1422+231: Each galaxy is part of a small group that contributes $\sim 10\%$ to the image separation (Hogg & Blandford 1994; Keeton & Kochanek 1997a; Kundić et al. 1997ab; Lehár et al. 1997; Schechter et al. 1997; Tonry 1997), and thus is expected to appear somewhat underluminous. With total magnitude estimates and a quantitative estimate of the correlation, it would be possible to see whether this is true.
- Q 0957+561: The galaxy is part of a cluster that contributes significantly to the large image separation (Young et al. 1980), so its position below the trend is expected.

With a good quantitative estimate of the image separation/lens luminosity correlation it would be possible to estimate the intrinsic image splitting of the galaxy, and thus to break the cluster degeneracy in lens models and estimates of the Hubble constant (see Grogin & Narayan 1996; Falco et al. 1997c; Fischer et al. 1997).

Table 6 gives the parameters M_{B^*} and γ derived from the correlations by fitting a subsample of lens galaxies, namely early-type galaxies with a known lens redshift (see the caption of Table 6 for a list). For each fit, a lens with both source and lens redshifts and a magnitude in only one passband was represented by a single data point. A lens with no source redshift or with magnitudes in multiple passbands was represented by two data points that cover the range of results from different passbands and/or different source redshifts ($2 \leq z_s \leq 4$). Rather than trying to estimate the uncertainties, we assumed uniform uncertainties scaled so that $\chi^2 = N_{dof}$ at the minimum. With this technique, the error bars give a rough estimate of the uncertainties from the observed scatter. The empirical correlations are at least broadly consistent with a Faber-Jackson coefficient $\gamma \approx 4$, although with the current data the values are slightly lower ($\gamma \simeq 2.7 \pm 0.5$ for $\Omega_0 = 1$). The values for M_{B^*} are also lower than the canonical value, but only by a few tenths of a magnitude.

Im et al. (1997) recently used the theoretical relation (eq. 3) with a sample of seven lens galaxies to constrain the cosmological model. They found that lens galaxy luminosities are significantly lower than expected unless λ_0 is large, which contradicts results from lens statistics (Maoz & Rix 1993; Kochanek 1996a; Falco et al. 1997a) that rule out a large λ_0 . We believe that the results of Im et al. (1997) are biased in two ways. First, Im et al. (1997) underestimated some of the lens galaxy magnitudes. For lenses with only aperture magnitudes, Im et al. (1997) subtracted 0.3 mag to estimate total magnitudes; we believe this to be a significant underestimate of the aperture corrections (compare Tables 3 and 4). In addition, Im et al. (1997) did not account for Galactic extinction, which is significant for several lenses (see Table 1). By using underestimated magnitudes, Im et al. (1997) forced the cosmological model to compensate by raising λ_0 to increase the luminosity inferred from a given apparent magnitude. Second, Im et al. (1997) did not properly treat the uncertainties in global parameters such as M_{B^*} . For example, for a canonical value of M_{B^*} with uncertainty σ_M , and a fitted value that differed by ΔM , Im et al. (1997) would have assigned $\Delta\chi^2 \simeq N_{lens}(\Delta M/\sigma_M)^2$ whereas a proper treatment of the covariance matrix would give $\Delta\chi^2 \simeq (\Delta M/\sigma_M)^2$. As a result, Im et al.’s (1997) cosmological uncertainties were underestimated by a factor of 2–3, independent of the systematic biases from underestimating the lens luminosities. Taking into account the underestimated luminosities and treating the uncertainties correctly overwhelms any cosmological conclusions. The image separation/lens luminosity correlation certainly promises to give an interesting

cosmological constraint, but only after the quality of the data has improved.

3.4. Mass-to-light ratios and galaxy evolution

Finally, we combined the masses from Table 5 with the aperture magnitudes from Table 4 to compute mass-to-light ratios. M/L estimates from lensing have a unique advantage over estimates from dynamical methods: whereas the dynamical methods are plagued by the ambiguities of using stellar dynamical models to estimate the mass, the lensing method has a robust mass estimate and thus is limited almost entirely by the quality of the photometry. In addition, because mass-to-light ratios depend only on aperture magnitudes and not on accurate profile fits and extrapolations, they yield physical results that are more reliable than the total luminosities studied in §3.3. As a result, lensing mass-to-light ratios offer an excellent probe of galaxy evolution and structure. Lensing also makes it possible to compute a reliable M/L estimate for individual galaxies, as opposed to M/L estimates from the fundamental plane that are usually interpreted only in a statistical sense.

Figure 7 shows the rest-frame B -band mass-to-light ratio inside the critical radius for the lens galaxies with a known lens redshift. These M/L_B use luminosities that were converted to rest-frame B by using the spectral evolution model to compute color and K corrections; we did *not* apply the evolutionary correction because we wanted to look for evidence of evolution. Note that although we are using V , R , and I magnitudes to compute the rest-frame B luminosity, we are not actually extrapolating the magnitudes; since rest-frame B is roughly equivalent to V at $z \simeq 0.2$ and I at $z \simeq 1$, we are in fact interpolating between magnitudes.

Although there is significant scatter in Figure 7, there is a clear decrease in M/L_B with redshift due to galaxy evolution. To lowest order, $\log M/L_B(z)$ is expected to be linear in z ,

$$\log M/L_B(z) = \log M/L_B(0) + z[d(\log M/L_B)/dz] + \dots \quad (4)$$

(e.g. van Dokkum & Franx 1996), so we can fit a line to the data. For the fit we excluded B 0218+357 because it is a spiral galaxy, B 1600+434 because it is poorly understood, and Q 0957+561 because the cluster mass makes the M/L something other than a true galaxy M/L . We used the same fit technique as in §3.3, with at most two data points per lens to represent the range of results, and uniform errors scaled to give $\chi^2 = N_{dof}$ at the minimum. Again the quoted error bars give a rough estimate of the uncertainties.

Table 6 summarizes the fits for the different cosmological models, and Figure 7 shows the best fits superposed on the data. We note that of the lens galaxies used in the fit, only

MG 0751+2716, PG 1115+080, and B 1422+231 lack estimates of the magnitude within the critical radius; we consider the fits both with and without these galaxies. Without these three galaxies, we find $d(\log M/L_B)/dz = -0.3 \pm 0.1$ for $\Omega_0 = 1$ and -0.5 ± 0.1 for $\Omega_0 = 0.1$ (with $\lambda_0 = 0$); including these galaxies gives evolution rates that are 1σ smaller. There is an additional systematic uncertainty because in this preliminary study we neglected the fact that M/L has a small dependence on luminosity (e.g. van der Marel 1991; Jørgensen, Franx & Kjørgaard 1996), and that with a dark matter lens model the M/L depends on the impact parameter. Our results are comparable to recent results from studies of intermediate-redshift clusters. Kelson et al. (1997) found $d(\log M/L_V)/dz \sim -0.3$ ($\Omega_0 = 0.1$) based on fundamental-plane observations of clusters at redshifts of 0.33, 0.39, and 0.58; and Schade et al. (1997) found $d(\log L)/dz \sim 0.3$ ($\Omega_0 = 1$) based on a projection of the fundamental plane in clusters at redshifts between 0.2 and 1. The fundamental plane studies are confined to galaxies in high-density clusters, but Stanford et al. (1997) suggest that evolution rates are not very sensitive to cluster properties such as optical richness or X-ray luminosity. The fact that we find similar evolution rates for lens galaxies in low-density environments provides further empirical evidence that there is no strong environmental dependence in the stellar populations of early-type galaxies.

Mass-to-light ratios are also important in setting the mass scale for both stellar dynamics and gravitational lensing. Previous studies have shown that consistency with constant M/L stellar dynamical models requires an average $M/L_B \sim (10 \pm 2)h$ (e.g. van der Marel 1991), while consistency with lens statistics requires $M/L_{B^*} = (20 \pm 4)h$ (e.g. Maoz & Rix 1993; Kochanek 1996a), and estimates from photometry and lens models of a few lenses have found $M/L_B \sim 20h$ (e.g. Kochanek 1995; Burke et al. 1992). Figure 8 shows the evolution-corrected M/L_B (i.e. where the rest-frame B luminosity has been estimated by applying the evolutionary correction in addition to the color, K , and Galactic extinction corrections) for our larger sample. Two lenses that have notably low values are B 0218+357, which is a spiral and has $M/L_B \sim 4h$ characteristic of spirals (e.g. Kent 1987; Broeils & Courteau 1997), and MG 0751+2716, which has only an isophotal magnitude that overestimates the luminosity within the critical radius and hence underestimates M/L_B . Other than these two lenses, the mass-to-light ratios are generally higher than expected from stellar dynamics, although they are somewhat lower than expected from lens statistics. The large scatter may be related to the dependence of M/L on luminosity and on impact parameter. With better photometric data and a larger lens sample it would be possible to correct for these effects to reduce the scatter, and thus to see whether they can explain why M/L from lens models might be smaller than those from lens statistics. Nevertheless, even at present the lens galaxy M/L provide weak evidence for dark matter in the inner regions of galaxies.

4. Conclusions

The sample of gravitational lens galaxies is now large enough to warrant a systematic study of their properties. By combining the available optical data, including new surface photometry of HST images, with constraints from lens models, we have surveyed the physical properties of 17 lens galaxies at redshifts between 0.1 and 0.8. Most of the galaxies appear to be passively evolving early-type galaxies, with the exception of one clear spiral (B 0218+357). Several lens galaxies (B 1600+434, B 1608+656, and B 1933+503) have poor-quality images or contamination from the lensed images and thus require further study to understand their colors and morphologies; nevertheless, at least for B 1608+656 and B 1933+503 the image separations, lens luminosities, and mass-to-light ratios are more consistent with early-type galaxies than with spirals. Several other lens galaxies (MG 0414+0534, MG 1131+0456, and HST 12531–2914) may or may not be anomalously red, depending on their redshifts. Our results do not support the suggestion by Malhotra et al. (1997) that massive galaxies at intermediate redshifts are very dusty, or by Jackson et al. (1997) that most of the lenses are spirals. Note that accepting either of these hypotheses would force a radical revision of almost all galaxy evolution models.

The shape distribution of lens galaxies is similar to that of the general population of early-type galaxies, although there is weak evidence for a deficit of apparently round lens galaxies; such a deficit may be created by the inclination dependence of lensing cross sections that bias flattened lens galaxies toward being viewed edge-on (Keeton & Kochanek 1997b). There is no obvious correlation between the optical and model ellipticities of lens galaxies. However, there is a strong correlation between the optical and model position angles, suggesting that the projected mass and projected light are generally aligned to $\lesssim 10^\circ$, except in the presence of strong external tidal perturbations. This conclusion rules out dark halos that are far out of equilibrium and have intrinsic axes misaligned with respect to the luminous baryons. It also suggests that halos cannot be formed solely by dissipationless collapse, because such halos tend to be very flat and nearly prolate (e.g. Dubinski & Carlberg 1991; Warren et al. 1992) so that, when they are combined with a typical modestly triaxial or oblate luminous galaxy (e.g. Franx et al. 1991), there is a large misalignment between the major axes of the projected mass and light (Romanowsky & Kochanek 1997). The interaction of the dark matter with the baryons must substantially alter the shape of the dark matter halo so that the light and mass have similar triaxialities and intrinsic axes, as is seen in the preliminary simulations of Dubinski (1994).

Lens galaxies obey the correlations between image separation and lens luminosity predicted by dark matter lens models combined with the Faber-Jackson and Tully-Fisher relations. For the early-type lens galaxies in an $\Omega_0 = 1$ cosmology, the characteristic

magnitude is $M_{B^*} = (-19.3 \pm 0.1) + 5 \log h$ and the “Faber-Jackson” exponent is $\gamma = 2.7 \pm 0.5$, with an additional systematic uncertainty due to uncertainties in total magnitude estimates, and to the uncertainty in σ_* from lens statistics (e.g. Fukugita & Turner 1991; Kochanek 1993a, 1996a). Im et al. (1997) attempted to use the image separation/lens luminosity correlation to constrain the cosmological model, but by underestimating aperture corrections, neglecting Galactic extinction, and improperly treating uncertainties they obtained misleading results favoring a high- λ_0 cosmology. A robust calculation of the image separation/lens luminosity correlation would offer an interesting cosmological constraint, but at present the data lack the necessary precision. The correlation would also improve the constraints on H_0 by allowing a calculation of the intrinsic image splitting of lens galaxies to break the cluster degeneracy in Q 0957+561 (see Grogin & Narayan 1996; Falco et al. 1997c; Fischer et al. 1997) and the group degeneracy in PG 1115+080 (see Schechter et al. 1997; Keeton & Kochanek 1997a; Courbin et al. 1997b), but again the required precision is not yet available. It might also be possible to search for the analog of the fundamental plane as an explanation of the scatter in the correlation, but the current sample has too few robust estimates of effective radii.

The most robust physical properties of the lens galaxies that we can calculate are mass-to-light ratios. Mass-to-light ratios require only aperture magnitudes, so they do not depend on accurate profile fits and extrapolations. In addition, lensing measures a mass that has an internal uncertainty of only a few percent (e.g. Kochanek 1991a; Wambsganss & Paczyński 1994) and systematic uncertainties of $\lesssim 20\%$ (due to external tidal perturbations, potential fluctuations associated with large-scale structure, or the cosmological model; e.g. Bar-Kana 1996; Wambsganss et al. 1997; Keeton et al. 1997). Thus lens galaxy mass-to-light ratios are limited primarily by the quality of the photometry, making them an outstanding probe of galaxy evolution. We measure an evolution rate of $d(\log M/L_B)/dz = -0.3 \pm 0.1$ (-0.5 ± 0.1) for $\Omega_0 = 1$ (0.1), although there is an additional systematic uncertainty M/L depends weakly on luminosity and more strongly on impact parameter in dark matter models, and in this preliminary study we did not include corrections. Our results for lens galaxies in low-density environments are comparable to results from measurements of the fundamental plane in intermediate-redshift clusters (e.g. Kelson et al. 1997; Schade et al. 1996, 1997), suggesting that there are no strong environmental effects in the evolution of early-type galaxies (see also Stanford et al. 1997). The evolution-corrected mass-to-light ratios help distinguish between early-type lens galaxies (which have $M/L_B \sim 10\text{--}20h$, e.g. van der Marel 1991; Maoz & Rix 1993; Kochanek 1996a) and spiral lens galaxies (which have $M/L_B \sim 4h$, e.g. Kent 1987; Broeils & Courteau 1997); at present, B 0218+357 is the only lens galaxy with a robust M/L_B estimate that is consistent with a spiral galaxy. For the early-type lens galaxies, the mass-to-light ratios are generally larger than expected

from constant M/L stellar dynamical models, although the scatter is large. Most of the scatter is due to uncertainties and systematic effects in the photometric data; in particular, it may be related to the dependence of M/L on luminosity and impact parameter. With improved photometric data the uncertainties would be significantly reduced, and lens galaxy mass-to-light ratios could provide strong evidence for dark matter in the inner parts of galaxies.

Our analysis is limited primarily by the quality of the optical data and by the absence of redshift measurements for some of the lens systems. Given a homogeneous data set with well-determined photometry, most of the observational uncertainties will be eliminated. Then by using its ability to probe mass distributions and measure masses – and thus to avoid difficult spectroscopy and dynamical analysis of distant galaxies – we can use gravitational lensing as a powerful probe of high-redshift galaxies and their evolution. In addition, with well-calibrated correlations it should be possible to use lens galaxy colors, luminosities, scale lengths, and image separations as an accurate method for estimating lens redshifts.

Acknowledgements: We thank J. Lehár, B. McLeod, E. Woods, and J. Huchra for useful discussions; in particular, J. Lehár and B. McLeod assisted with the analysis of several lens systems. Support for this work was provided by the Smithsonian Institution, and by NASA through grant number 05505 from the Space Telescope Science Institute, which is operated by the Association of Universities for Research in Astronomy, Inc., under NASA contract NAS5-26555. CRK is supported by ONR-NDSEG grant N00014-93-I-0774. CSK is supported by NSF grant AST-9401722 and NASA ATP grant NAG5-4062.

REFERENCES

- Bar-Kana, R. 1996, *ApJ*, 468, 17
- Bender, R., Ziegler, B., & Bruzual, G. 1996, *ApJ*, 463, L51
- Bernstein, G., Fischer, P., Tyson, J. A., Rhee, G. 1997, *ApJ*, 483, L79 (Be97)
- Broeils, A. H., & Courteau, S. 1997, in *Dark and Visible Matter in Galaxies*, ed. M. Persic & P. Salluci (San Francisco: ASP) (also preprint astro-ph/9610264)
- Browne, I. W. A., Patnaik, A. R., Walsh, D., & Wilkinson, P. N. 1993, *MNRAS*, 263, L32 (Br93)

- Browne, I. W. A., et al. 1997, in *Observational cosmology with the new radio surveys*, ed. M. Bremer, N. Jackson & I. Perez-Fournon (Dordrecht: Kluwer) (Br97)
- Bruzual, G., & Charlot, S. 1993, *ApJ*, 405, 538
- Buote, D. A., & Canizares, C. R. 1994, *ApJ*, 427, 86
- Buote, D. A., & Canizares, C. R. 1996, *ApJ*, 457, 177
- Burke, B. F., Lehár, J., & Conner, S. R. 1992, in *Gravitational Lenses*, ed. R. Kayser, T. Schramm & L. Nieser (Berlin: Springer), 237
- Cardelli, J. A., Clayton, G. C., & Mathis, J. S. 1989, *ApJ*, 345, 245
- Carilli, C. L., Rupen, M. P., & Yanny, B. 1993, *ApJ*, 412, L59
- Chen, G. H., & Hewitt, J. N. 1993, *AJ*, 106, 1719 (Ch93)
- Chen, G. H., Kochanek, C. S., & Hewitt, J. N. 1995, *ApJ*, 447, 62 (Ch95)
- Crampton, D., Le Fèvre, O., Hammer, F., & Lilly, S. J. 1996, *A&A*, 307, 53 (Cr96)
- Combes, F., & Wiklind, T. 1997, preprint astro-ph/9706274
- Courbin, F., Lidman, C., & Magain, P. 1997a, preprint astro-ph/9707183
- Courbin, F., Magain, P., Keeton, C. R., Kochanek, C. S., Vanderriest, C., Jaunsen, A. O., & Hjorth, J. 1997b, *A&A*, in press (also preprint astro-ph/9705093) (Co97)
- de Vaucouleurs, G. 1948, *Ann d'Ap*, 11, 247
- Djorgovski, S., & Davis, M. 1987, *ApJ*, 313, 59
- Dressler, A., Lynden-Bell, D., Burstein, D., Davies, R. L., Faber, S. M., Terlevich, R. J., Wegner, G. 1987, *ApJ*, 313, 42
- Dubinski, J., & Carlberg, R. G. 1991, *ApJ*, 378, 496
- Dubinski, J. 1994, *ApJ*, 431, 617
- Efstathiou, G., Ellis, R. S., & Peterson, B. A. 1988, *MNRAS*, 232, 431
- Eisenhardt, P. R., Armus, L., Hogg, D. W., Soifer, B. T., Neugebauer, G., & Werner, M. W. 1996, *ApJ*, 461, 72
- Ellis, R. S. 1997, *ARA&A*, 35, in press (also preprint astro-ph/9704019)

- Fabbiano, G., 1989, *ARA&A*, 27, 87
- Faber, S. M., & Jackson, R. E. 1976, *ApJ*, 204, 668
- Falco, E. E., Gorenstein, M. V., & Shapiro, I. I. 1985, *ApJ*, 289, L1
- Falco, E. E., Kochanek, C. S., & Muñoz, J. A. 1997a, *ApJ*, in press (also preprint astro-ph/9707032)
- Falco, E. E., Lehár, J., & Shapiro, I. 1997b, *AJ*, 113, 540 (F197)
- Falco, E. E., Shapiro, I. I., Moustakas, L. A., & Davis, M. 1997c, *ApJ*, 484, 70
- Fassnacht, C. D., Womble, D. S., Neugubauer, G., Browne, I. W. A., Readhead, A. C. S, Matthews, K., & Pearson, T. J. 1996, *ApJ*, 460, L103 (Fs96)
- Fischer, P., Bernstein, G., Rhee, G., & Tyson, J. A. 1997, *AJ*, 113, 521
- Franx, M., Illingworth, G., & de Zeeuw, T. 1991, *ApJ*, 383, 112
- Fukugita, M., & Turner, E. L. 1991, *MNRAS*, 253, 99
- Fukugita, M., Shimasaku, K., & Ichikawa, T. 1995, *PASP*, 107, 945
- Gebhardt, K., et al. 1996, *AJ*, 112, 105
- Gorenstein, M. V., Shapiro, I. I., & Falco, E. E. 1988, *ApJ*, 327, 693
- Griffiths, R. E., et al. 1994, *ApJ*, 437, 67
- Grogin, N. A., & Narayan, R. 1996, *ApJ*, 464, 92; erratum, 1996, *ApJ*, 473, 570
- Guiderdoni, B., & Rocca-Volmerange, B. 1987, *A&A*, 186, 1
- Guiderdoni, B., & Rocca-Volmerange, B. 1988, *A&AS*, 74, 185
- Hammer, F., Le Fèvre, O., Angonin, M. C., Meylan, G., Smette, A., & Surdej, J. 1991, *A&A*, 250, L5
- Hewitt, J. N., Turner, E. L., Schneider, D. P., Burke, B. F., Langston, G. I., & Lawrence, C. R. 1988, *Nature*, 333, 537 (He88)
- Hewitt, J. N., Turner, E. L., Lawrence, C. R., Schneider, D. P., & Brody, J. P. 1992, *AJ*, 104, 3 (He92)
- Hogg, D. W., & Blandford, R. D. 1994, *MNRAS*, 268, 889

- Holtzman, J. A., Burrows, C. J., Casertano, S., Hester, J. J., Trauger, J. T., Watson, A. M., & Worthey, G. 1995, *PASP*, 107, 1065
- Huchra, J., Gorenstein, M., Kent, S., Shapiro, I., Smith, G., Horine, E., & Perley, R. 1985, *AJ*, 90, 691
- Im, M., Griffiths, R. E., & Ratnatunga, K. U. 1997, *ApJ*, 475, 457
- Impey, C. D., Foltz, C. B., Petry, C. E., Browne, I. W. A., & Patnaik, A. R. 1996, *ApJ*, 462, L53 (Im96)
- Jackson, N., et al. 1995, *MNRAS*, 274, L25 (Jc95)
- Jackson, N., Nair, S., & Browne, I. W. A. 1997, in *Observational cosmology with the new radio surveys*, ed. M. Bremer, N. Jackson & I. Perez-Fournon (Dordrecht: Kluwer) (Jc97)
- Jaunsen, A. O., & Hjorth, J. 1997, *A&A*, 317, L39
- Jørgensen, I., & Franx, M. 1994, *ApJ*, 433, 553
- Jørgensen, I., Franx, M., & Kjærgaard, P. 1996, *MNRAS*, 280, 167
- Kassiola, A., & Kovner, I. 1993, *ApJ*, 417, 459
- Keeton, C. R., & Kochanek, C. S. 1996, in *Astrophysical Applications of Gravitational Lensing*, ed. C. S. Kochanek & J. N. Hewitt (Dordrecht: Kluwer), 419
- Keeton, C. R., & Kochanek, C. S. 1997a, *ApJ*, in press (also preprint astro-ph/9611216)
- Keeton, C. R., & Kochanek, C. S. 1997b, *ApJ*, in press (also preprint astro-ph/9705194)
- Keeton, C. R., Kochanek, C. S., & Seljak, U. 1997, *ApJ*, 482, 604
- Kelson, D. D., van Dokkum, P. G., Franx, M., Illingworth, G. D., & Fabricant, D. 1997, *ApJ*, 478, L13
- Kent, S. M. 1987, *AJ*, 93, 816
- King, L. J., & Browne, I. W. A. 1996, *MNRAS*, 282, 67
- Kochanek, C. S. 1991a, *ApJ*, 373, 354
- Kochanek, C. S. 1991b, *ApJ*, 379, 517

- Kochanek, C. S. 1992, *ApJ*, 384, 1
- Kochanek, C. S. 1993a, *ApJ*, 419, 12
- Kochanek, C. S. 1993b, *MNRAS*, 261, 453
- Kochanek, C. S. 1994, *ApJ*, 436, 56
- Kochanek, C. S. 1995, *ApJ*, 445, 559
- Kochanek, C. S. 1996a, *ApJ*, 466, 638
- Kochanek, C. S. 1996b, *ApJ*, 473, 595
- Kormann, R., Schneider, P., & Bartelmann, M. 1994a, *A&A*, 284, 285
- Kormann, R., Schneider, P., & Bartelmann, M. 1994b, *A&A*, 286, 537
- Kormendy, J., & Djorgovski, S. 1989, *ARA&A*, 27, 235
- Krist, J. 1997, *The Tiny Tim User's Manual v. 4.3*, STScI
- Kristian, J., et al. 1993, *AJ*, 106, 1330 (Kr93)
- Kundić, T., Cohen, J. G., Blandford, R. D., & Lubin, L. M. 1997a, preprint astro-ph/9704109 (Ku97a)
- Kundić, T., Hogg, D. W., Blandford, R. D., Cohen, J. G., Lubin, L. M., & Larkin, J. E. 1997b, preprint astro-ph/9706169 (Ku97b)
- Kurucz, R. L. 1979, *ApJS*, 40, 1
- Langston, G. I., Schneider, D. P., Conner, S., Carilli, C. L., Lehar, J., Burke, B. F., Turner, E. L., Gunn, J. E., Hewitt, J. N., & Schmidt, M. 1989, *AJ*, 97, 1283 (Ln89)
- Langston, G. I., Conner, S. R., Lehar, J., Burke, B. F., & Weiler, K. W. 1990, *Nature*, 344, 43 (Ln90)
- Lawrence, C. R., Schneider, D. P., Schmidt, M., Bennett, C. L., Hewitt, J. N., Burke, B. F., Turner, E. L., & Gunn, J. E. 1984, *Science*, 223, 46
- Lawrence, C. R., Elston, R., Jannuzi, B. T., & Turner, E. L. 1995, *AJ*, 110, 2570 (Lw95)
- Lawrence, C. R. 1996, in *Astrophysical Applications of Gravitational Lensing*, ed. C. S. Kochanek & J. N. Hewitt (Dordrecht: Kluwer), 299 (Lw96)

- Lehár, J., Langston, G. I., Silber, A., Lawrence, C. R., & Burke, B. F. 1993, *AJ*, 105, 847 (Le93)
- Lehár, J., Cooke, A. J., Lawrence, C. R., Silber, A. D., & Langston, G. I. 1996, *AJ*, 111, 1812 (Le96)
- Lehár, J., Burke, B. F., Conner, S. R., Falco, E. E., Fletcher, A. B., Irwin, M., McMahon, R. G., Muxlow, T. W. B., & Schechter, P. L. 1997a, preprint astro-ph/9702191 (Le97a)
- Lehár, J., et al. 1997b, in preparation (Le97b)
- Lilly, S. J., Tresse, L., Hammer, F., Crampton, D., & Le Fèvre, O. 1995, *ApJ*, 455, 108
- Lin, H., Kirshner, R. P., Shectman, S. A., Landy, S. D., Oemler, A., Tucker, D. L., & Schechter, P. L. 1996, *ApJ*, 464, 60
- Lin, H., Yee, H. K. C., Carlberg, R. G., & Ellingson, E. 1997, *ApJ*, 475, 494
- Malhotra, S., Rhoads, J. E., & Turner, E. L. 1997, *MNRAS*, 288, 138
- Maoz, D., & Rix, H.-W. 1993, *ApJ*, 416, 425
- Marlow, D. R., Sykes, C. M., Nair, S., Jackson, N. J., Browne, I. W., Wilkinson, P. A., de Bruyn, A. G., Myers, S. T., & Fassnacht, C. D. 1997, in *Golden Lenses: The Hubble Constant and Galaxies at High Redshift* (available at <http://multivac.jb.man.ac.uk:8000/ceres/workshop1/proceedings.html>) (Ma97)
- McLeod, B. 1997, private communication (Ml97)
- McMahon, R., Irwin, M., & Hazard, C. 1992, *Gemini*, 36, 1 (Mm92)
- Myers, S. T., et al. 1995, *ApJ*, 447, L5 (My95)
- Nair, S., & Garrett, M. A. 1997, *MNRAS*, 284, 58
- Ostriker, J. P., & Peebles, P. J. E. 1973, *ApJ*, 186, 467
- Pahre, M. A., Djorgovski, S. G., & de Carvalho, R. R. 1996, *ApJ*, 456, L79
- Patnaik, A. R., Browne, I. W. A., Walsh, D., Chaffee, F. H., & Foltz, C. B. 1992, *MNRAS*, 259, 1P (Pa92)
- Patnaik, A. R., Browne, I. W. A., King, L. J., Muxlow, T. W. B., Walsh, D., & Wilkinson, P. N. 1993, *MNRAS*, 261, 435 (Pa93)

- Patnaik, A. R., Porcas, R. W., & Browne, I. W. A. 1995, MNRAS, 274, L5 (Pa95)
- Perna, R., Loeb, A., & Bartelmann, M. 1997, ApJ, in press (also preprint astro-ph/9705172)
- Poggianti, B. M. 1997, A&AS, 122, 399
- Ratnatunga, K. U., Ostrander, E. J., Griffiths, R. E., & Im, M. 1995, ApJ, 453, L5 (Ra95)
- Rix, H.-W. 1991, Ph.D. Thesis, University of Arizona,
- Rix, H.-W., de Zeeuw, P. T., Carollo, C. M., Cretton, N., & van der Marel, R. P. 1997, preprint astro-ph/9702126
- Romanowsky, A. J., & Kochanek, C. S. 1997, ApJ, in press
- Sackett, P. D., Rix, H.-W., Jarvis, B. J., & Freeman, K. C. 1994, ApJ, 436, 629
- Sackett, P. D. 1996, in *Astrophysical Applications of Gravitational Lensing*, ed. C. S. Kochanek & J. N. Hewitt (Dordrecht: Kluwer), 165
- Salpeter, E. E. 1955, ApJ, 121, 161
- Scalo, J. M. 1986, FunCosP, 11, 1
- Schade, D., Lilly, S. J., Crampton, D., Hammer, F., Le Fèvre, O., & Tresse, L. 1995, ApJ, 451, L1
- Schade, D., Carlberg, R. G., Yee, H. K. C., & López-Cruz, O. 1996, ApJ, 464, L63
- Schade, D., Barrientos, L. F., & López-Cruz, O. 1997, ApJ, 477, L17
- Schechter, P. L. 1976, ApJ, 203, 297
- Schechter, P. L., et al. 1997, ApJ, 475, L85
- Spitzer, L. 1978, *Physical Processes in the Interstellar Medium* (New York: Wiley), 156
- Stanford, S. A., Eisenhardt, P. R., & Dickinson, M. 1997, preprint astro-ph/9708037
- Stark, A. A., Gammie, C. F., Wilson, R. W., Bally, J., Linke, R. A., Heiles, C., & Hurwitz, M. 1992, ApJS, 79, 77
- Surdej, J., Magain, P., Swings, J.-P., Borgeest, U., Courvoisier, T. J.-L., Kayser, R., Kellermann, K. L., Kühr, H., & Refsdal, S. 1987, Nature, 329, 22 (Su87)
- Tomita, K. 1996, PASJ, 48, 265

- Tonry, J. L. 1997, preprint astro-ph/9706199 (To97)
- Tully, R. B., & Fisher, J. R. 1977, *A&A*, 54, 661
- Turner, E. L., Ostriker, J. P., & Gott, J. R. 1984, *ApJ*, 284, 1
- van der Marel, R. P. 1991, *MNRAS*, 253, 710
- van Dokkum, P. G., & Franx, M. 1996, *MNRAS*, 281, 985
- Walsh, D., Carswell, R. F., & Weymann, R. J. 1979, *Nature*, 279, 381 (Wa79)
- Wambsganss, J., Cen, R., Xu, G., & Ostriker, J. P. 1997, *ApJ*, 475, L81
- Wambsganss, J., & Paczyński, B. 1994, *AJ*, 108, 1156
- Warren, M. S., Quinn, P. J., Salmon, J. K., Zurek, W. H. 1992, *ApJ*, 399, 405
- Weymann, R. J., Latham, D., Angel, F. R. P., Green, R. F., Liebert, J. W., Turnshek, D. A., Turnshek, D. E., & Tyson, J. A. 1980, *Nature*, 285, 641 (We80)
- Wiklind, T., & Combes, F. 1995, *A&A*, 299, 382
- Wisotski, L., Köhler, T., Kayser, R., & Reimers, D. 1993, *A&A*, 278, L15
- Witt, H. J., & Mao, S. 1997, preprint astro-ph/9702021
- Young, P., Gunn, J. E., Kristian, J., Oke, J. B., & Westphal, J. A. 1980, *ApJ*, 241, 507 (Yo80)

Table 1. Gravitational Lens Geometries, Galactic Extinctions, and Redshifts

Name	Geometry [§]	$E(B - V)$ [#]	z_s	z_l	Reference
Q 0142–100	Double (O)	0.05	2.72	0.49	Su87
B 0218+357	Double+Ring (R, O)	0.10	0.96	0.68	Pa93, Br93, Lw96
MG 0414+0534	Quad+Arc (R, O)	0.18	2.64	$0.44_{0.15}^{0.85\dagger}$	He92, Lw95
B 0712+472	Quad (R, O)	0.15	1.33	0.41	Br97
MG 0751+2716	Ring (R)	0.07		0.35	Le97
BRI 0952–0115	Double (O)	0.07	4.5	$0.99_{0.31}^{1.96\dagger}$	Mm92
Q 0957+561	Double (R, O)	0.01	1.41	0.36	Wa79, Yo80
PG 1115+080	Quad (O)	0.06	1.72	0.31	We80, Ku97a, To97
MG 1131+0456	Ring+Arc (R, O)	0.06			He88
HST 12531–2914	Quad (O)	0.10			Ra95
HST 14176+5226	Quad (O)	0.02	$(3.4)^\dagger$	0.81	Ra95, Cr96
B 1422+231	Quad (R, O)	0.04	3.62	0.34	Pa92, Ku97b, To97
MG 1549+3047	Ring (R)	0.04		0.11	Le93
B 1600+434	Double (R, O)	0.02	1.57	0.41	Jc95, Br97
B 1608+656	Quad+Arc (R, O)	0.05	1.39	0.63	My95, Fs96
MG 1654+1346	Ring (R)	0.09	1.74	0.25	Ln89
B 1933+503	Quad ^{**} (R)	0.16		0.76	Br97

[§]Ring indicates a ring of lensed extended radio emission, and arc indicates lensed extended optical emission. Double or quad indicates two or four images. R and O indicate whether the lensed images have been detected at radio and optical wavelengths.

^{**}B 1933+503 has a complicated geometry with as many as 10 images. It appears to consist of three sources, two of which are quadruply imaged and one of which is doubly imaged (Browne et al. 1997).

[#]Galactic extinction, in magnitudes, computed by estimating the HI column density N_H from Stark et al. (1992) and then converting to $E(B - V)$ using $N_H/E(B - V) = 5.9 \times 10^{21} \text{ mag}^{-1} \text{ cm}^{-2}$ from Spitzer (1978).

[†](\dots) denotes a tentative measurement of the source redshift.

[‡]Estimated median lens redshift and 90% confidence interval (for an $\Omega_0 = 1$ cosmology), computed from the probability of producing the observed image separation (see Kochanek 1992).

Table 2. Lens Galaxy Structural Parameters and Colors

Name	R_e (arcsec)	e	PA ($^\circ$)	Filters	Color	Method, Ref
Q 0142–100	(0.50 ± 0.03)	0.31 ± 0.03	63 ± 4	F555W, F675W	1.57	B, new
B 0218+357				F555W, F814W	2.10	A, Jc97, MI97
MG 0414+0534	1.28 ± 0.09	0.29 ± 0.04	81 ± 4	F675W, F814W	1.51	B, Fl97
B 0712+472	(0.42 ± 0.04)	0.59 ± 0.03	60 ± 2	F555W, F814W	2.09	B, Jc97
MG 0751+2716	(0.27 ± 0.03)	0.49 ± 0.03	17 ± 2	R		A, Le97
BRI 0952–0115	(0.14 ± 0.03)	0.43 ± 0.08	61 ± 7	F675W		B, new
Q 0957+561	4.63 ± 0.07	0.21 ± 0.01	49 ± 2	F555W, F814W	1.82	B, Be97
PG 1115+080				F785LP		Kr93
MG 1131+0456	0.90 ± 0.08	0.12 ± 0.04	36 ± 10	F675W, F814W	1.25	B, new
HST 12531–2914	0.19 ± 0.02	0.17 ± 0.05	20 ± 8	F606W, F814W	2.11	B, Ra95
HST 14176+5226	1.13 ± 0.05	0.30 ± 0.02	37 ± 2	F606W, F814W	2.19	B, Ra95
B 1422+231	(0.8 ± 0.2)	0.27 ± 0.13	-59 ± 15	F342W, F480LP	(2.0)	A, Im96
MG 1549+3047	(3.5)	0.35 ± 0.05	-40 ± 5	V, I	(1.3)	A, Le93, Le96
B 1600+434		(0.4 ± 0.1)	45 ± 5	F555W, F814W	(2.35)	B/C, Jc97
B 1608+656	(0.39 ± 0.04)	0.60 ± 0.03	81 ± 2	F555W, F814W	(2.00)	B/C, Jc97
MG 1654+1346	1.80 ± 0.02	0.40 ± 0.01	-83 ± 1	F675W, F814W	0.65	B, new
B 1933+503		(0.57 ± 0.03)	-41 ± 2	F555W, F814W	(2.30)	B/C, Jc97

Note. — Each lens galaxy is described by its effective radius R_e , ellipticity $e = 1 - b/a$, major axis position angle, and color. The colors have not been corrected for Galactic extinction. The methods are as follows: (A) Results taken from the cited literature. (B) Results determined from an elliptical de Vaucouleurs profile fit to HST images; results based on archival images cite the first known publication of the observations, and results based on our new observations are listed as “new.” (C) Color determined inside an $0''.3$ radius aperture centered on the galaxy. Error bars are standard errors using a χ^2 rescaled to be unity per degree of freedom at the minimum. Formal uncertainties for the colors from profile fits are negligible, but systematic uncertainties are probably ~ 0.2 mag. (\dots) denotes a value that is systematically uncertain because the galaxy is too faint or its light is significantly affected by the lensed images (see text). Structural parameters left blank were unavailable in the literature and/or impossible to determine reliably from HST images; colors left blank indicate that observations were available in only one passband.

Table 3. Lens Galaxy Total Magnitudes

Name	F814W	F675W	F555W	Other		Method
Q 0142–100		19.26	20.83			B
B 0218+357	(20.0)		(22.0)			A
MG 0414+0534	20.50	22.01				B
B 0712+472	19.48		21.57			B
MG 0751+2716				(R)	[21.3]	A
BRI 0952–0115		21.89				B
Q 0957+561	16.43		18.24			B
PG 1115+080				(F785LP)	[18.4]	A
MG 1131+0456	20.76	22.01				B
HST 12531–2914	21.42			(F606W)	23.54	B
HST 14176+5226	19.53			(F606W)	21.72	B
B 1422+231				(F480LP)	[21.6]	(F342W) [23.6] A
MG 1549+3047				(I)	[16.3]	(V) [17.6] A
B 1600+434	[20.4]					B
B 1608+656	[19.7]		[22.7]			B
MG 1654+1346	17.46	18.10				B
B 1933+503	[21.9]					B

Note. — The magnitudes have not been corrected for Galactic extinction. Method A: magnitudes taken from the literature. Method B: total magnitudes determined from elliptical de Vaucouleurs profile fits. Formal uncertainties for the magnitudes from profile fits are negligible, but systematic uncertainties are probably ~ 0.2 mag. (\dots) denotes a magnitude that is uncertain by an estimated 0.5 mag, while $[\dots]$ denotes a magnitude that has no aperture correction and thus underestimates the total magnitude. The references are the same as in Table 2.

Table 4. Lens Galaxy Aperture Magnitudes

Name	F814W	F675W	F555W	Other		Method	
Q 0142–100		19.54	21.11			B	
B 0218+357	(21.4)		(23.7)			A	
MG 0414+0534	21.19	22.70				B	
B 0712+472	19.82		21.90			B	
MG 0751+2716				(R)	[21.3]	A	
BRI 0952–0115		22.03				B	
Q 0957+561	17.35		19.17			B	
PG 1115+080				(F785LP)	[18.4]	A	
MG 1131+0456	21.45	22.70				B	
HST 12531–2914	21.67			(F606W)	23.77	B	
HST 14176+5226	20.06			(F606W)	22.24	B	
B 1422+231				(F480LP)	[21.6]	(F342W) [23.6]	A
MG 1549+3047				(I)	(17.8)	(V) (19.1)	A
B 1600+434	(21.4)		(23.9)			B	
B 1608+656	(19.7)		(22.7)			B	
MG 1654+1346	18.44	19.09				B	
B 1933+503	(21.9)					B	

Note. — Magnitudes measured inside a circular aperture with radius equal to the critical radius (b_{SIS}) of the lens models in Table 5. They have not been corrected for Galactic extinction. Method A: magnitudes taken from the literature. Method B: magnitudes determined from elliptical de Vaucouleurs profile fits. Formal uncertainties for the magnitudes from profile fits are negligible, but systematic uncertainties are probably ~ 0.2 mag. (\dots) denotes a magnitude that is uncertain by an estimated 0.5 mag, while $[\dots]$ denotes an aperture magnitude whose aperture radius is not equal to the critical radius. The references are the same as in Table 2.

Table 5. Singular Isothermal Lens Models

Name	b_{SIS} (")	γ	b_{SIE} (")	e	PA ($^\circ$) [†]	χ^2/N_{dof} [‡]	Ref
Q 0142–100	1.17 ± 0.05	0.08 ± 0.02	1.14 ± 0.02	0.21 ± 0.05	76_{-18}^{+9}	(0) 0/0	HST ^a
B 0218+357	0.17						Pa95 ^d
MG 0414+0534	1.18 ± 0.03	0.10 ± 0.03	1.14 ± 0.03	0.38 ± 0.09	79 ± 1	(116)111/6	Ka97
B 0712+472	0.69 ± 0.02	0.05 ± 0.04	0.69 ± 0.01	0.25 ± 0.11	50 ± 1	(28) 24/6	HST
MG 0751+2716	0.40	0.09	0.41	0.34	64		Le97a ^b
BRI 0952–0115	0.52 ± 0.01	0.07 ± 0.01	0.51 ± 0.01	0.19 ± 0.03	65 ± 5	(0) 0/0	HST
Q 0957+561			3.09	0.64	69 ± 1		Le97b ^b
PG 1115+080	1.14 ± 0.01	0.12 ± 0.02	1.08 ± 0.03	0.48 ± 0.07	67 ± 1	(250)483/6	Co97
MG 1131+0456	0.92 ± 0.01	0.11 ± 0.01	0.92	0.33	–26		Ch95 ^b Ch93
HST 12531–2914	0.55 ± 0.03	0.15 ± 0.05	0.54 ± 0.04	0.38 ± 0.17	19 ± 4	(20) 35/6	Ra95
HST 14176+5226	1.42 ± 0.06	0.15 ± 0.04	1.34 ± 0.09	0.52 ± 0.11	49 ± 3	(96)111/6	Ra95
B 1422+231	0.77 ± 0.01	0.26 ± 0.01	0.65 ± 0.02	0.63 ± 0.03	-53 ± 1	(40)124/6	Pa92, Im96
MG 1549+3047			1.15	0.07	–48		Le93 ^b
B 1600+434	0.70						Jc95 ^d
B 1608+656	1.10 ± 0.03	0.06 ± 0.04	1.07 ± 0.04	0.35 ± 0.16	69 ± 2	(837)790/6	HST
MG 1654+1346	0.98 ± 0.01	0.08 ± 0.01	0.98	0.27	–81		Ko95 ^b Ln90
B 1933+503	0.50 ± 0.01	0.15 ± 0.02	0.45 ± 0.01	0.60 ± 0.03	-46 ± 1	(10) 3/4	Ma97 ^c

[†]Major-axis PA for the SIE lens models. The PAs for the SIS+shear models are the same to within the error bars.

[‡]The χ^2 for the SIS+shear and SIE models, and the number of degrees of freedom, in the form: $(\chi_{SIS}^2 \chi_{SIE}^2) / N_{dof}$.

^aHST denotes a model based on data from our analysis of the HST images.

^bModel results taken from the literature.

^cThe χ^2 for B 1933+503 is deceptively low. The image position error bars σ_p were not given in Marlow et al. (1997), so actually $\chi_{SIE}^2 = 3(0''.01/\sigma_p)^2$ (and similar for χ_{SIS}^2). In addition, the models used only the quadruply-imaged flat spectrum source and neglected the other lensed images.

^dCritical radius estimated from a singular isothermal sphere lens model to produce the observed image separation.

Note. — Results from singular isothermal sphere plus external shear (SIS+shear; b_{SIS} and shear γ) and singular isothermal ellipsoid (SIE; b_{SIE} and ellipticity e) lens models, based on data from the cited literature. Point-image lenses were modeled by fitting the quasar image positions and flux ratios as well as the galaxy position if available (e.g. Keeton & Kochanek 1997a). Radio rings were modeled using the LensClean program (e.g. Kochanek 1995; Chen et al. 1995). The error bars are 1σ standard errors using a χ^2 renormalized to equal N_{dof} at the minimum; because the models generally are poor fits, these error bars overestimate the mass uncertainties. The SIS model gives a robust estimate for the mass within the critical radius, $M = \pi b^2 \Sigma_{cr}$, which depends only weakly on the lens model. The ellipticity depends on the radial mass profile of the lens, roughly as $(1 - \kappa_r)$ where κ_r is the surface density of the model at the critical radius in units of the critical surface density – more centrally concentrated models require higher ellipticities. The position angle is essentially model-independent in single-shear models.

Table 6. Empirical Results

(Ω_0, λ_0)	$M_{B^*} - 5 \log h^\dagger$	γ^\dagger	$\log M/L_B(0)^\ddagger$	$d(\log M/L_B)/dz^\ddagger$
(1.0, 0.0)	-19.3 ± 0.1	2.7 ± 0.5	(1.09) 1.15 ± 0.04	(-0.24) -0.31 ± 0.08
(0.1, 0.0)	-19.4 ± 0.1	3.3 ± 0.4	(1.13) 1.19 ± 0.04	(-0.40) -0.47 ± 0.08
(0.4, 0.6)	-19.6 ± 0.1	3.2 ± 0.4	(1.10) 1.17 ± 0.05	(-0.45) -0.53 ± 0.08
(0.2, 0.8)	-20.0 ± 0.1	3.7 ± 0.5	(1.11) 1.17 ± 0.05	(-0.57) -0.64 ± 0.08

[†] Fits to the lens luminosity/image separation correlations in §3.3, using the early-type lens galaxies with a known lens redshift (0142, 0712, 0751, 1115, 14176, 1422, 1549, 1608, 1654, and 1933). Including 0957 in the fits gives results that are statistically consistent with those in the table. Error bars were computed assuming uniform errors scaled so that $\chi^2 = N_{dof}$ at the minimum.

[‡] Fits to the mass-to-light ratio evolution in §3.4. The results in parentheses use all of the early-type lens galaxies with a known lens redshift (listed above). The other results exclude 0751, 1115, and 1422 because these lens galaxies lack accurate estimates of the magnitude within the critical radius. Again error bars were computed assuming uniform uncertainties scaled so that $\chi^2 = N_{dof}$ at the minimum.

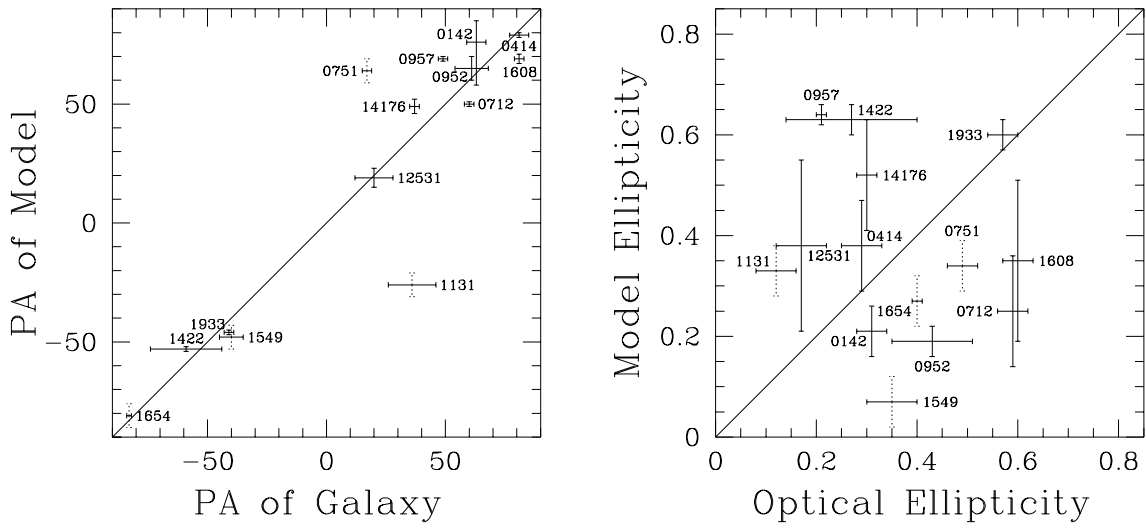


Fig. 1.— Observed and model PAs and ellipticities, from Tables 2 and 5. For model results with no formal error bars, we use error bars of 5° in the PA and 0.05 in e and indicate them by dotted lines.

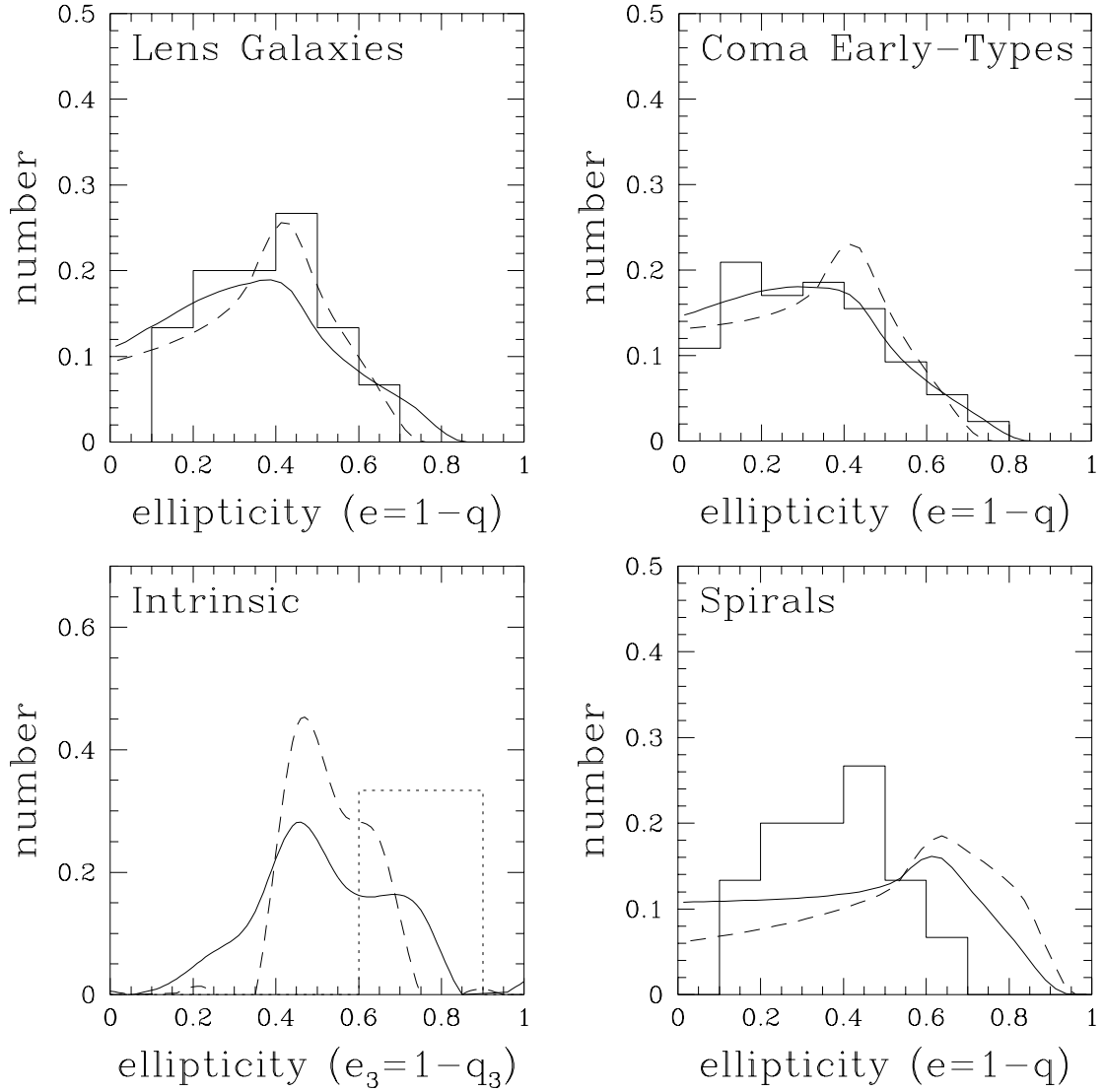


Fig. 2.— Optical ellipticity distribution of lens galaxies and of a sample of early-type galaxies in Coma (Jørgensen & Franx 1994), where q is the projected axis ratio and q_3 is the intrinsic axis ratio. The histograms in the upper left and upper right show the lens galaxy and Coma samples, respectively. In the lower left, the solid and dashed curves show deprojections of the Coma and lens galaxy samples, respectively, assuming galaxies are oblate. In the upper left and right, the curves show reprojections of the deprojected distributions. Note that the lensing projection and deprojection take into account the effects of both inclination bias (Keeton & Kochanek 1997b) and magnification bias (Falco et al. 1997a). Finally, the lower right shows the effects expected for spirals. Specifically, an (assumed) intrinsic distribution given by the dotted line in the lower left projects to the curves in the lower right, where the solid curve is a simple projection and the dashed curve is a lensing projection. The lens galaxy histogram is included for comparison.

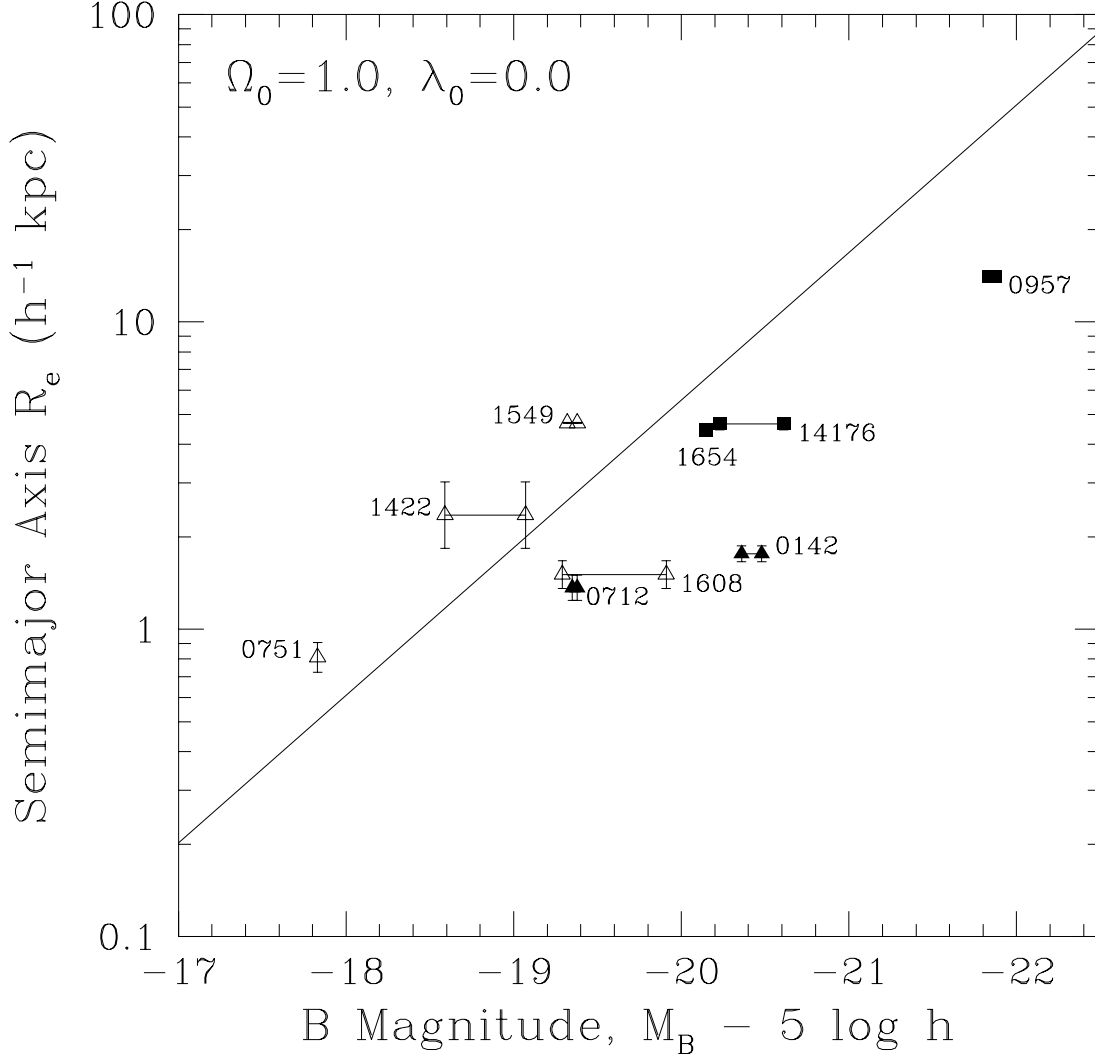


Fig. 3.— Luminosities and scale lengths for lens galaxies in an $\Omega_0 = 1$ cosmology. Filled (open) symbols denote luminosities computed from total (aperture) magnitudes combined with color, K , evolution, and Galactic extinction corrections. Points connected by a horizontal line denote magnitudes from multiple passbands. Squares (triangles) denote robust (uncertain) estimates for R_e . The solid line shows the correlation for nearby early-type galaxies, $R_e/R_{e*} = (L/L_*)^a$ with $R_{e*} = (4 \pm 1)h^{-1}$ kpc and $a = 1.2 \pm 0.2$ (e.g. Kormendy & Djorgovski 1989; Rix 1991).

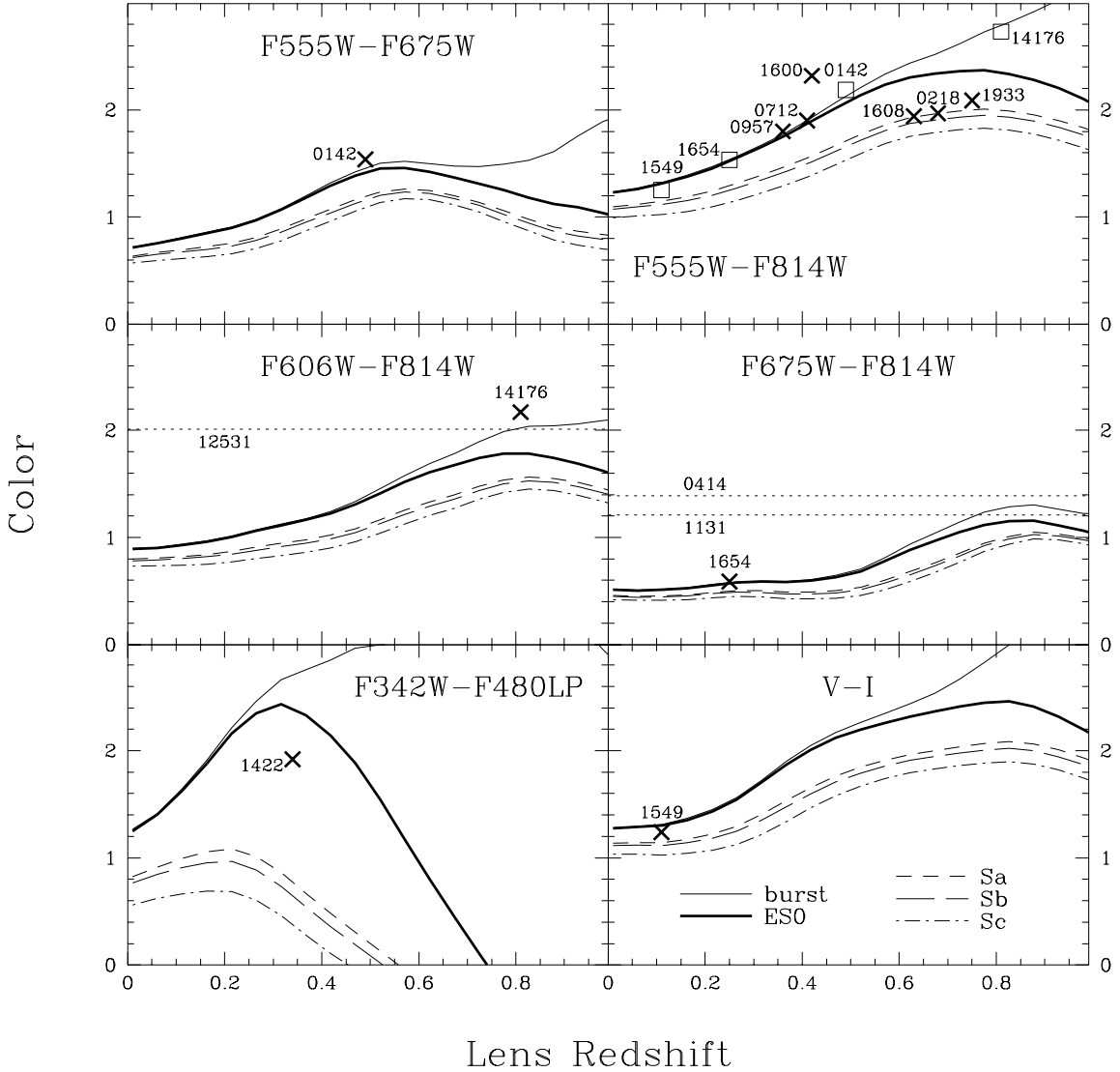


Fig. 4.— Observed extinction-corrected colors and theoretical color evolution curves. Lens galaxies with a known redshift are shown as crosses, while those with no known redshift are shown as horizontal dotted lines. For 0142, 14176, 1549, and 1654, we estimated F555W–F814W colors by applying color transformations to the observed colors; these points are shown as boxes. Theoretical color evolution curves are shown for various galaxy types: the “burst” model consists of a 1 Gyr period of constant star formation followed by passive evolution; the E/S0 model has an exponential star formation rate with a time scale of 1 Gyr; and the spiral models have a star formation rate proportional to the gas fraction, where the proportionality constant decreases from Sa to Sb to Sc (see Guiderdoni & Rocca-Volmerange 1988). The burst and E/S0 models have a Salpeter (1955) IMF, while the spiral models have a Scalo (1986) IMF. The curves shown are for $\Omega_0 = 1$ and $H_0 = 50 \text{ km s}^{-1} \text{ Mpc}^{-1}$, with a galaxy formation redshift $z_f = 15$.

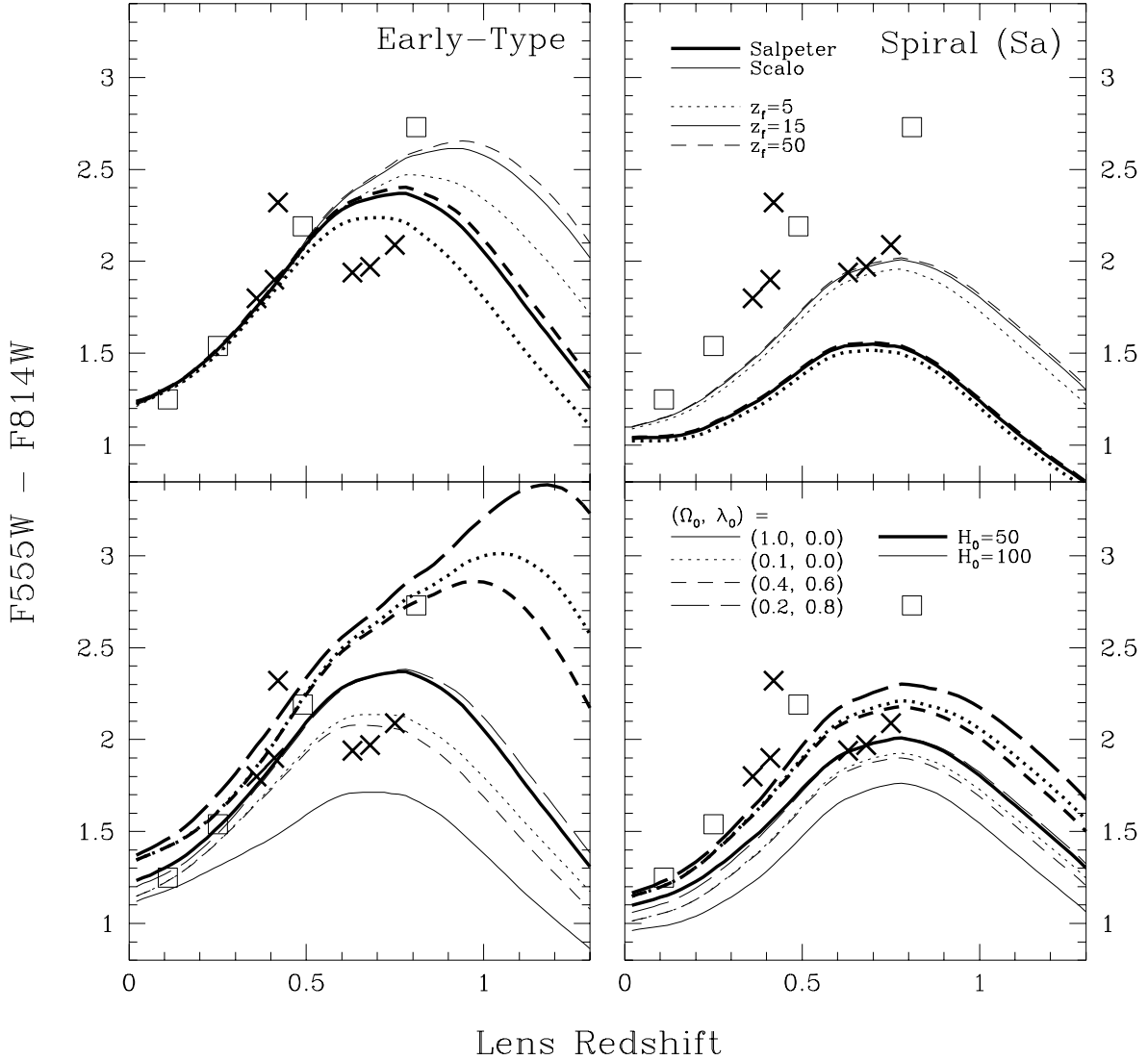


Fig. 5.— Systematic effects in the theoretical color evolution curves for early-type (left) and spiral (right) galaxy models. In all panels the crosses and boxes denote observed or estimated extinction-corrected F555W–F814W colors taken from Figure 4. *Top*: The effects of changing the galaxy evolution model. The heavy curves have a Salpeter (1955) IMF while the light curves have a Scalo (1986) IMF. The dotted, solid, and dashed lines have a formation redshift $z_f = 5, 15,$ and 50 , respectively. The cosmological model is $\Omega_0 = 1$ and $H_0 = 50$ km s⁻¹ Mpc⁻¹. *Bottom*: The effects of changing the cosmological model. The heavy (light) curves have $H_0 = 50$ (100) km s⁻¹ Mpc⁻¹. The solid, dotted, and dashed curves have different values for Ω_0 and λ_0 . All curves have $z_f = 15$, so the present galaxy ages are $12.8 h_{50}^{-1}$ Gyr ($\Omega_0 = 1$), $17.0 h_{50}^{-1}$ Gyr ($\Omega_0 = 0.1$ or $\lambda_0 = 0.6$), and $20.6 h_{50}^{-1}$ Gyr ($\lambda_0 = 0.8$).

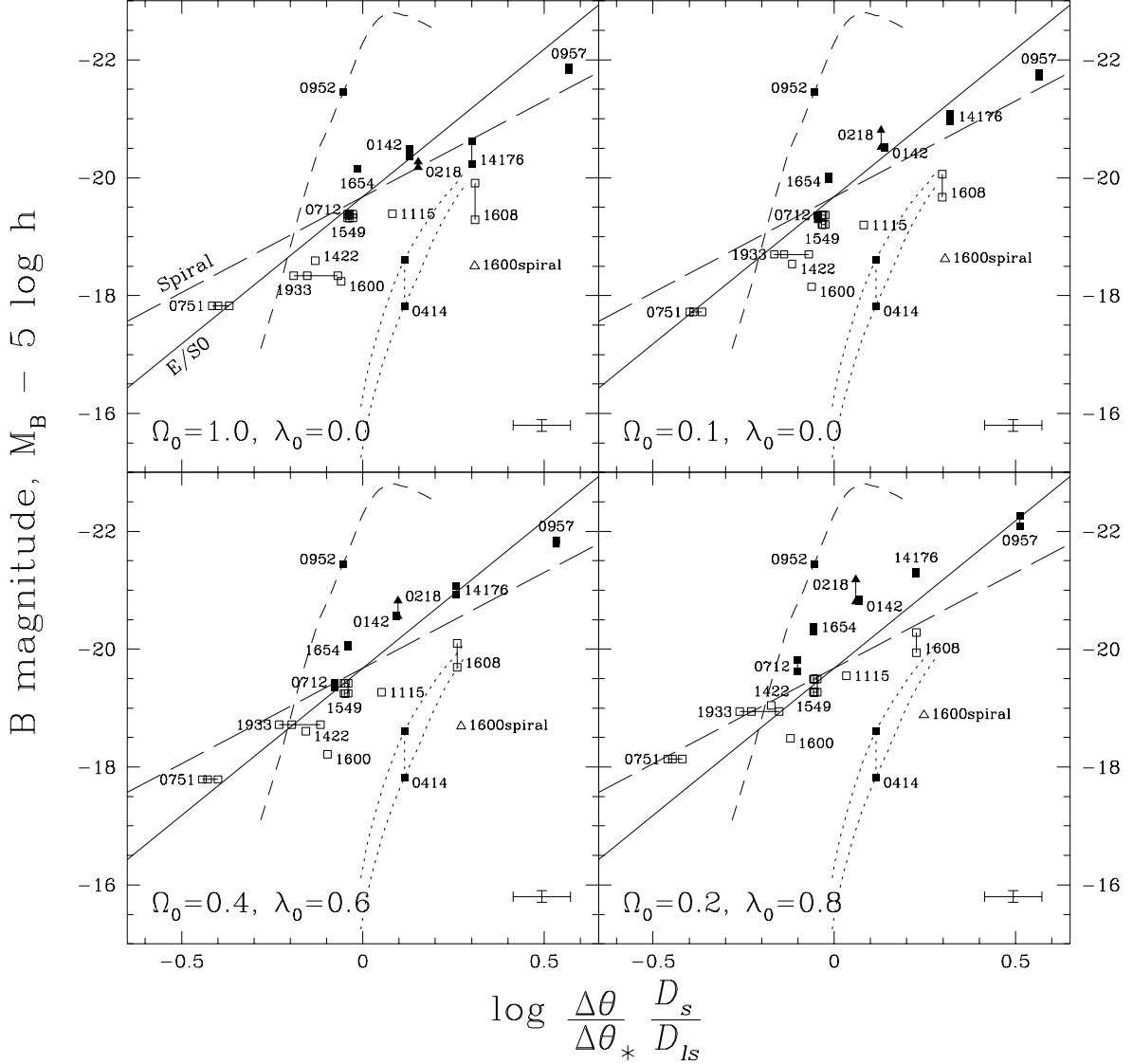


Fig. 6.— Image separation/lens luminosity correlations. The horizontal axis is the normalized separation using $\Delta\theta = 2b_{SIS}$ with b_{SIS} from Table 5. The vertical axis is the rest-frame absolute B magnitude using total magnitudes from Table 3 with color, K , evolutionary, and Galactic extinction corrections. Filled points denote plausible total magnitudes and open points denote aperture magnitudes. Triangles denote spirals and squares denote early-types. Where the lens redshift is unknown, the points indicate the median expected redshift and the lines indicate the 90% confidence interval (see Table 1). Where the source redshift is unknown, points along the horizontal line denote $z_s = 2, 3,$ and 4 (from right to left). Lenses with magnitudes in multiple bands are represented by points connected vertically. The expected relations for E/S0 and spiral galaxies are shown by the solid and dashed lines. The error bars indicate the uncertainties in $\Delta\theta_*$ and M_{B*} .

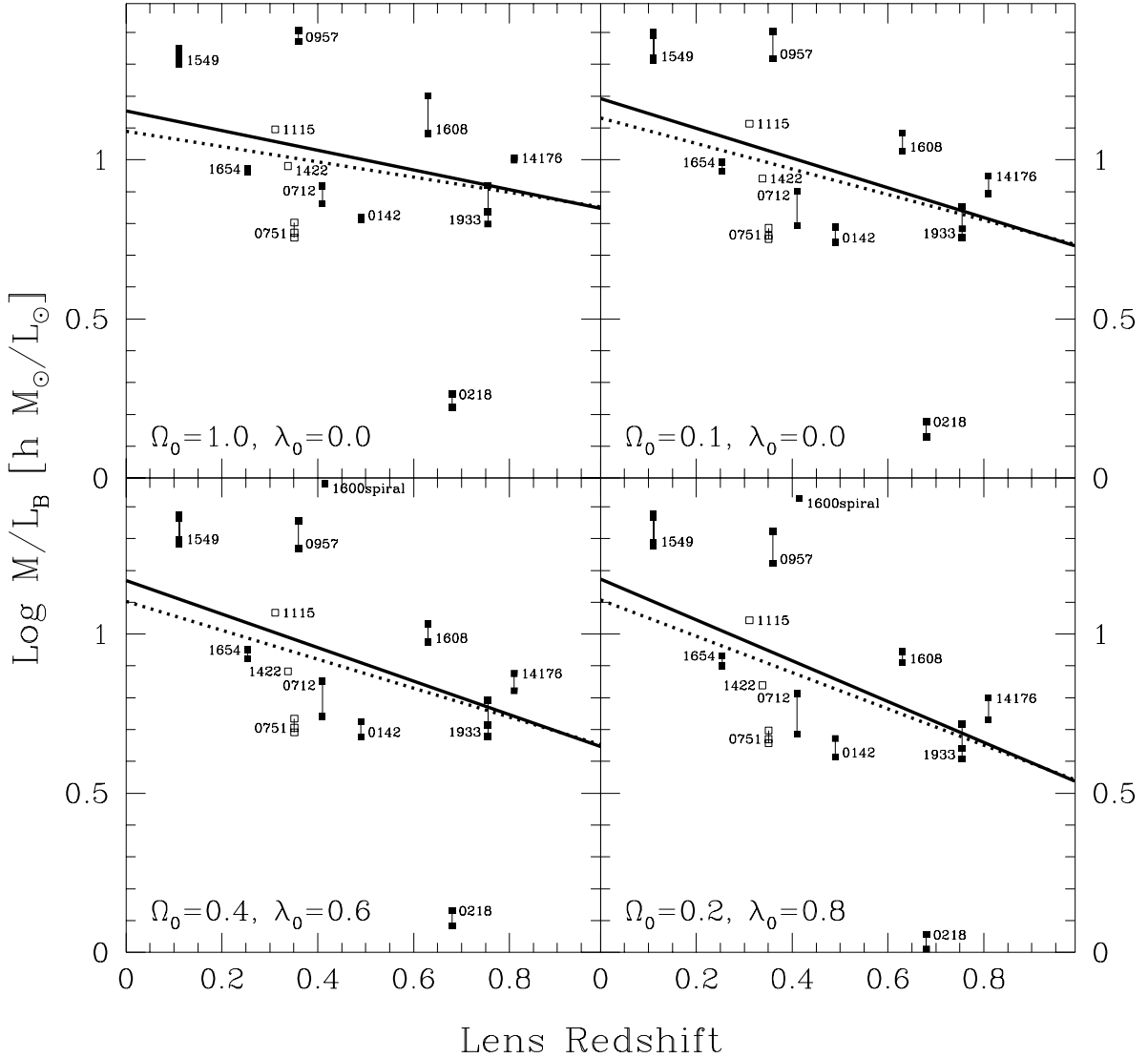


Fig. 7.— Rest-frame B -band mass-to-light ratios inside the critical radius. The luminosities were computed from the aperture magnitudes in Table 4 with Galactic extinction, color, and K corrections – *but no evolutionary corrections*. Filled points indicate that the aperture magnitudes used an aperture radius equal to the critical radius, while open points indicate an aperture radius not equal to the critical radius. Vertical lines connect values of M/L computed from different photometric bands, and (for 0751, 1549, and 1933) with different source redshifts ($z_s = 2, 3,$ and 4); thus the spread in the points gives some idea of the systematic uncertainties. 0218 stands out because it is a spiral galaxy, and 0957 because the mass from the cluster increases the M/L ; 1600 is off the scale in the two upper panels. The clear trend of M/L with redshift is consistent with passive evolution. The heavy lines show the best fits to this trend; the solid lines exclude 0751, 1115, and 1422 from the fits, while the dotted lines include them (see the text and Table 6).

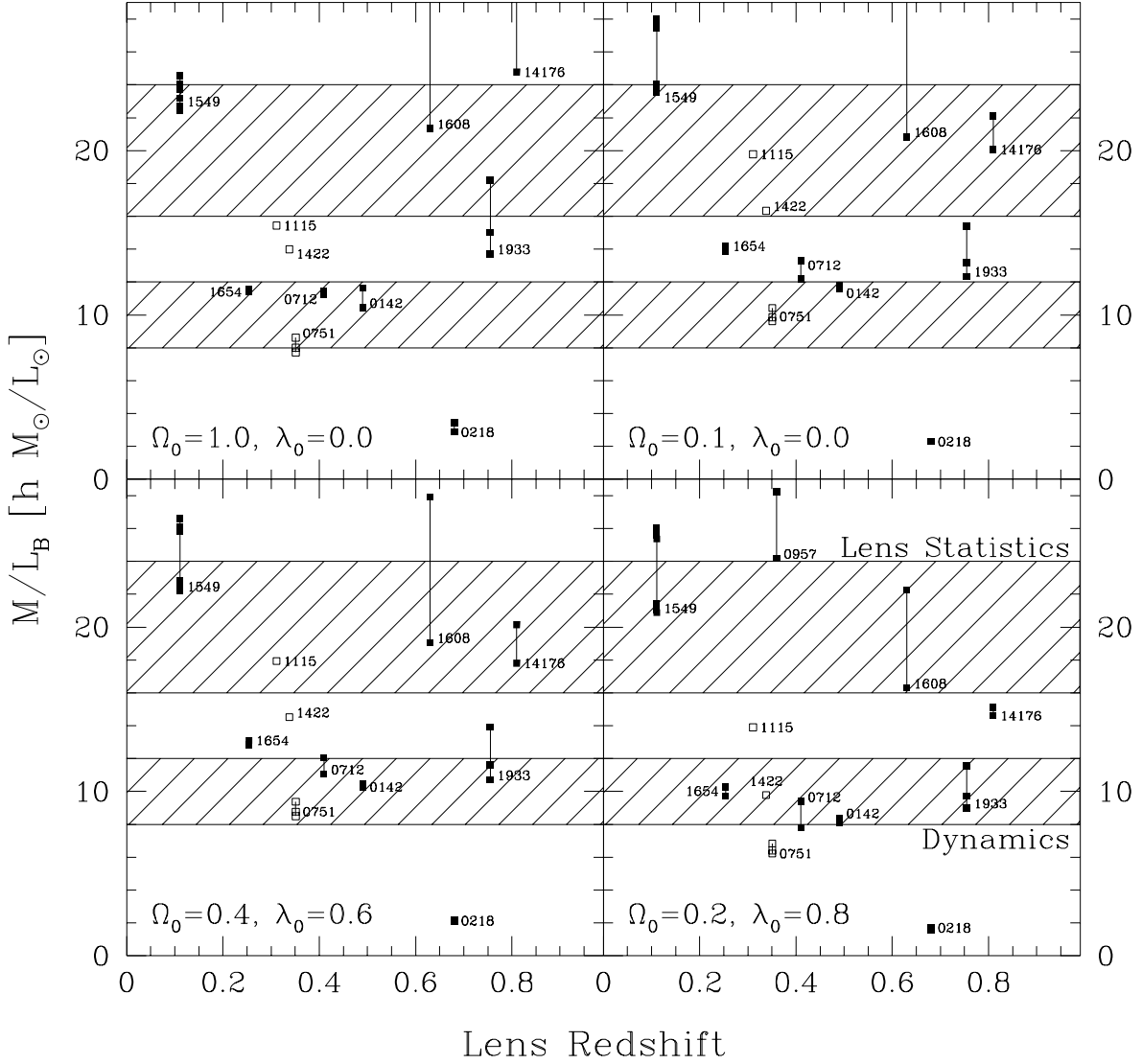


Fig. 8.— Evolution-corrected M/L , i.e. the same M/L as in Figure 7 except that the evolutionary correction has been added. The notation is the same as in Figure 7. Again 0218 stands out because it is a spiral, and 0957 (which is off the scale in all but the $\lambda_0 = 0.8$ panel) because the mass from the cluster increases the M/L . The shaded regions indicate the results from lens statistics (e.g. Maoz & Rix 1993; Kochanek 1996a) and from constant M/L stellar dynamical models (e.g. van der Marel 1991).